UNIVERSITY OF COPENHAGEN
FACULTY OF SCIENCE

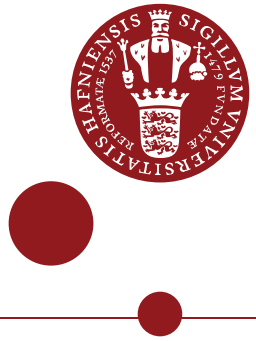

A thesis presented to the Faculty of Science in partial fulfillment of the requirements for the degree

Master of Science in Nanoscience

Bio- and Medical Physics specialization

Investigation of Poly-aneuploid cancer cells motility in 3D

Hazal Polat

hvg644@ku.dk

August 2022

Supervisors: Liselotte Jauffred and Veneta Gerganova

Submitted on: 8 August 2022

Acknowledgements

I would like to thank Associate Professor Liselotte Jauffred, for giving me the opportunity to work on this project and being an amazing supervisor. Thanks for always having an open door for questions and offering weekly meetings. Also, thank you for being so in tune with your students' conditions and willing to accommodate changes during the stressful time of this project.

My deep appreciation is also extended to post doc and Dr. Veneta Gerganova for the support. Veneta taught me how to be in a cell lab as I have not been in a cell lab before - additionally she has been a huge help to getting me started with her project. Thanks for all the explanations on to the biology behind the project, that was really needed as it is still a new field. Although I only had the pleasure of Veneta's presence for the first 2 months, she was always ready to help me if I had any questions about the experiments, the lab or biology. Last, a big thanks to her again at the end of the project in putting things together and helping me to go through this period mentally even she got her little baby Kai in the meantime.

I would also like to thank Prof. Dr. Emma Hammarlund and her lab from University of Lund for the collaboration and support. Thank you, Emma, for forcing me to give the talks at Lund University and John Hopkins University. Thanks for ordering material which was needed for the project.

Thanks to Ph.D. student, Mireia Cordero Sánchez – for helping me with python and plots, and thanks for the needed explanation on the physics side of this project.

Thanks to the Experimental biophysics group and the Ph.D. office with the coolest people.

Lastly, I want to thank my family. My dad, my mom and little brother for always being there for me. They helped me to have faith. Thank you for believing in me.

Abstract:

Poly-aneuploid cancer cells, otherwise known as PACCs, are a novel and exciting single cell system for cancer biology research presenting a great opportunity as a highly relevant cell type to advance cancer treatment therapies. PACCs are large, multinucleated chemotherapy resistant survivor cancer cells, which exhibit motile behaviors on 2D substrates, making them a highly likely candidate for metastatic cell precursors. In this project I study and describe the migration phenotypes of PACCs exhibited in physiologically relevant 3D substrates. I implemented 3D encapsulation and live microscopy approaches to challenge these cancer-derived cells and study their behavior in environments that more closely resemble the challenges encountered *in vivo*. The results of the investigation indicate that the PACCs switch from active motility in 2D to more a static, but still exploratory behavior using filopodia in 3D. The large PACCs seem unable to freely transverse the presented 3D gel environment in which the cell is encapsulated. These intriguing results merit a re-visit of the original hypothesis, which postulated that if the cells are motile on 2D substrates, they could potentially exhibit similar motility in 3D environments. I discuss the relevance of the results of this study in the context of the currently known cell biology of the PACCs and I propose new directions for future work.

Table of contents

ACRONYMS

ECM Extracellular Matrix

PACCs Poly-aneuploid Cancer Cells

PGCCs Poly-giant cancer cells

WGD Whole Genome Doubling

PC3 Prostate Cancer Cell Line

MPF Maturation Promoting Factor

DMEM Dulbecco's Modified Eagle's Medium

FBS Fetal Bovine Serum

PBS Phosphate Buffered Saline

MEM Minimum Essential Medium

RCF Relative Centrifugal Force

MSD Mean Squared Displacement

EA MSD Ensemble averaged MSD

Introduction

Living organisms across the tree of life display various behaviors as a response to their environment. The behavior is often recognized as movement, for example towards food sources upon recognizing changes in nutrient availability, or away from threats. While such behaviors are easily observable in higher order organisms, studying them down to molecular detail is often too complex. Single cell systems provide a great analytical tool to address how environmental stimuli are perceived and how they can trigger a behavioral response such as movement. More specifically, the research project presented in this thesis focuses on how single cells perceive changes in their *physical* environment and how in turn that causes a change in the *dynamic behavior* of those cells.

Several cell types exhibit dynamic behaviors, or movement, which is essential to their important functions in various tissues. For example, dendritic cell migration for antigen presentation [1], keratinocytes in wound repairing [2,3] macrophages and leukocytes in the immune system [4], or metastasizing cancer cells [5].

Here, I am investigating the effects of the physical environment on cell motility in the field of cancer biology. Namely, how individual chemotherapy resistant cancer cells develop and display motility in 3D environments, an essential process to be studied in order to understand cancer metastases.

1 Theoretical Background:

1.2 Cancer

Cancers are defined as uncontrolled tissue growth caused by the uncontrolled division of individual cancer cells, which are an abnormally altered cell type. Generally, cancer cells show deregulated proliferation, which is the process of a cell dividing and growing in the same stage. To achieve uncontrolled proliferation healthy cells, undergo various mutations and therefore modifications of their cell shape and function. The accumulation of such modified cells results in the formation of growing tissue masses known as tumors. The biggest hazard with cancer progression is not particularly tumor formation itself, since tumors can remain benign [6], but rather the formation of cancer metastases when individual cells move and proliferate in new parts of the body [7,8,9]. In the worst case, untreated metastases and invasion can continue and spread almost everywhere in the human body. Around 90% of all cancer deaths are caused by the spread of the cancer instead of the primary tumor itself. [5]

This makes cancer metastasis an incredibly important process to investigate in detail. The current knowledge on the cancer spreading process is that it occurs in the following steps: [9] (See Figure 1)

1) Metastasis and invasion: The cascade begins with tumor cells migrating away from the primary tumor through invasion of the barriers of the surrounding extracellular matrix (ECM).
2) Intravasation or entrance of tumor cells into blood vessels or the lymphatic system through the membrane.
3) Cells travel through the bloodstream. Here, a tumor cell's ability to survive in the bloodstream circulation is determined by its ability to resist stress. [9]
4) Tumor cells enter secondary sites after attaching to newly reached blood vessels, also known as extravasation.
5) Lastly, the cancer cells start to colonize the new location.

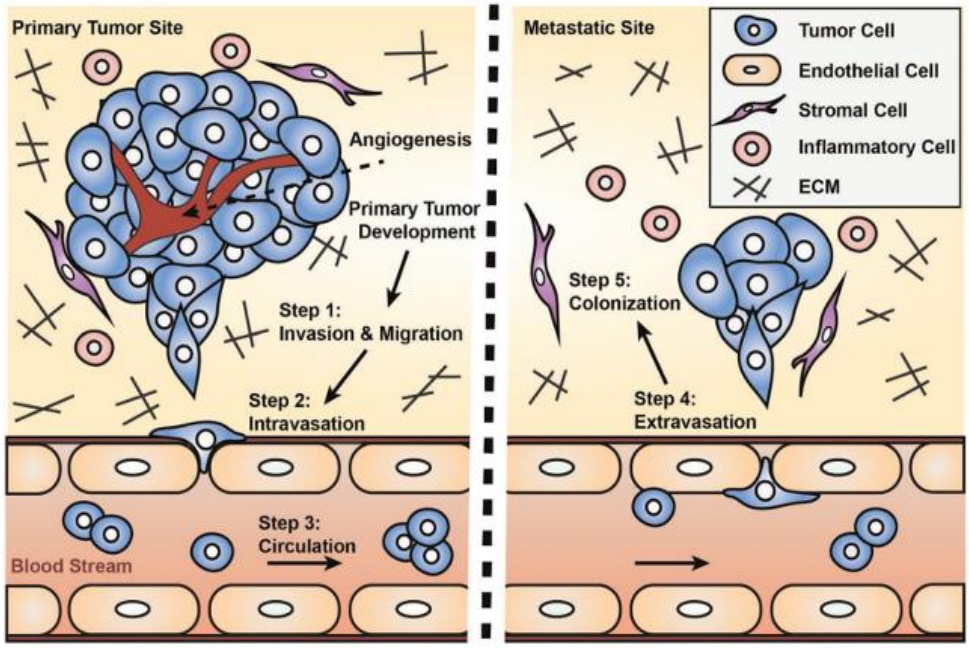

Figure 1: An illustration of the five steps a tumor cell undergoes from the primary tumor to a secondary location. Figure is from [9].

The metastatic pathway clearly demonstrates that during the spreading away from the primary location, a cancer cell has to adapt to a series of various environments. Both at the primary tumor location, during the metastatic movement, and at the new location, the cancer cells have to detect and respond to widely different microenvironments, each of which will result in a different behavioral response [10]. Therefore, in this work we investigate how the physical environment will affect the behavior of a particular cancer cell type, which we describe in more details below.

1.2.1 Chemotherapy

Chemotherapy is a standard treatment for cancer patients and has given a huge advancement to cancer treatment since the 20th century. It is performed through the use of chemical compounds which target cancer cells [11]. Not always chemotherapy can ensure the full recovery of a patient and the complete elimination of every cancer cell. Some cells appear to resist the treatment and later continue proliferating at the site of the primary tumor or in a new location. For example, the cancer cell type we use for the current investigation, known as poly-aneuploid cancer cells (PACCs) are generated post chemotherapy; they remain resistant to the original treatment and later in their life cycle they produce daughter cells resistant to the original treatment [12]. In this project, cisplatin is used as a chemical compound to simulate chemotherapy *in vitro* for the generation of PACCs. Cisplatin is a commonly used chemical compound synthesized by M. Peyrone in 1844. The chemical structure makes it possible to bind

cancer cell DNA, causing DNA damage and interfering with DNA repair thereby resulting in cell death [13,14].

1.3 Poly-aneuploid cancer cells, PACCs

In this investigation of the development of motility as a response to the environment, we have selected a unique and highly relevant single cell system: *Poly-aneuploid cancer cells (PACCs)*. PACCs are a rare type of cancer cell newly under the spotlight after a series of research efforts demonstrated that this cell type could serve as a precursor of treatment-resistant metastasizing cancer cells [12]. PACCs were first observed in an *in vitro* system developed for live microscopy imaging of the effects of various treatments on a collection of cancer cell lines [15]. The first tested treatment was a gradient of hypoxic environment where the majority of the precursor cancer cells died, however a small percentage of cells remained resistant to the treatment (about 5%). Among the resistant cells were a mix of cells with size similar to the original cell line called "sister cells" as well as individual cells that had significantly larger size than the original cancer cell line sizes (PACCs). Those large cells carried either an enlarged single nucleus or were multinucleated. Initially these cells were considered pre-apoptotic, however, surprisingly under continued live-cell microscopy of about 14 days, instead of going through cell death, they began displaying motile behaviors about four to five days post treatment. After 10-14 days, the PACCs were also able to produce treatment-resistant motile daughter cells through cell division and/or budding. This process is remarkably robust since PACCs' generation described here was possible for multiple cell lines. Six different cancer lines were tested also under other types of stress such as pH changes, absence of nutrients, chemotherapy, or radiation. Remarkably, the generated PACCs and their progeny are resistant not only to the originally supplied chemotherapy drug, but to the other described stresses as well. Empirically, it was established that the induction of the PACCs was correlated to the dose of treatment with higher stress producing more PACCs [12,15,16,17,18,19].

This cancer cell behavior is unique and highly relevant to the study of cancer metastases, so it raises the question, why weren't these cell types observed and reported on previously? A closer look into various publications shows that these cells were visible in many images from *in vitro* cell culture and histology preparations from patient biopsies (Figure 2). However, as previously stated, due to their morphology and size they were discussed solely as pre-apoptotic. As the current investigations show, these cells are also not very common, they amount to below 5% of treated populations, so they are difficult to capture without a protocol dedicated to their enriched generation. The development of modern technologies for observation of live cells in microscopy

for long periods while simultaneously supplying treatments are allowing us to fully describe the chain of events that these cells encounter [12,16,17,18,19].

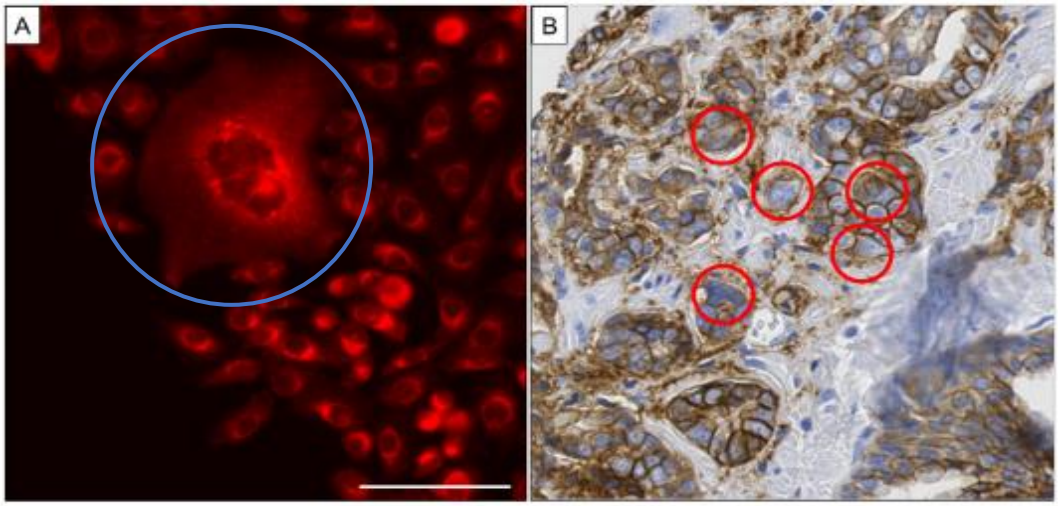

Figure 2: Different environments PACCs have been found in. A) The blue circle shows a PACC (from cell culture) stained with Nile Red contrast B) Red circles shows PACCs clinically found in prostate cancer from a patient. The Figure is from [17].

How do these cells reach such an increase in cell size and what does it mean for their functionality?

Originally these cells were named poly-giant cancer cells (PGCCs) due to the visual observation of their size. Closer investigation of their molecular processes led to the better description of their genetics. Since all cancer cells in general are aneuploid, this includes the cell type described here. What separates them from other cancer cells, is that they carry an n+ aneuploidy which is the reason why they are called poly-aneuploid cancer cells or PACCs. PACCs undergo whole genome doubling (WGD) without subsequent cell division and in this way retain an increasingly higher number of chromosomal materials, which can happen in a single enlarged nucleus or in multiple nuclei. The need to preserve the nuclear-cytoplasmic ratio in all living cells means that the higher genetic content results in increases of the cytoplasm and needed organelles, ultimately resulting in a misshapen morphology (Figure 3) [20]. The final PACC size depends on which parent cell line they are derived from with originally smaller cell sizes producing somewhat smaller PACCs [12,16,17,18,19,21]. Due to the lack of cell division, it can be described that the PACCs have entered a quiescent-like state, where they are retaining proliferative potential, but have exited the cell cycle.

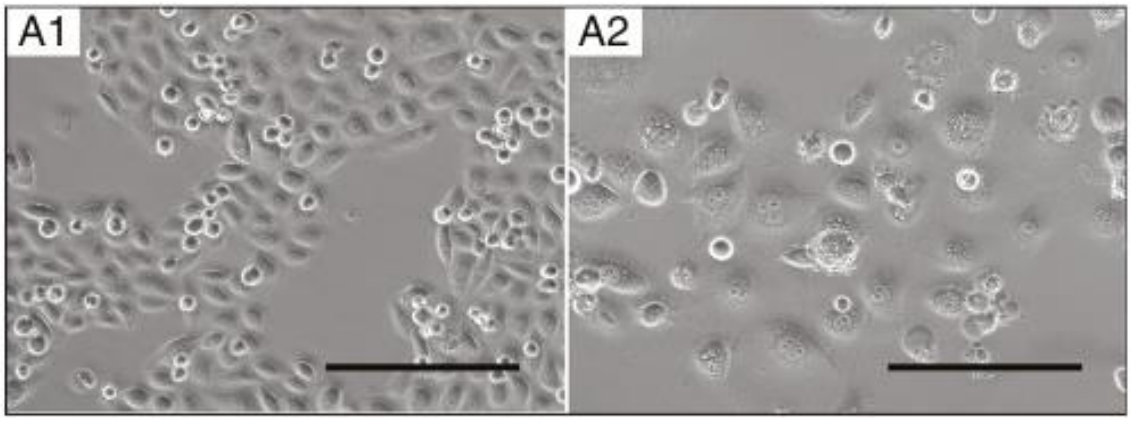

Figure 3: PACCs are found in the PC3 cell line. A) The PC3 cell line not treated with chemotherapy and B) shows an example of how the PACCs can be formed after 72 h treatment. The figure is from [12].

To retain the ability to grow while withstanding stress, the PACCs demonstrate different metabolism with increased fat stores and lipid droplets. Figure 4 shows that PACCs are full of lipid containing structures, with the PACCS potentially using these fat stores for survival post-stress. While stress is present the fat stores allow them to remain dormant [21].

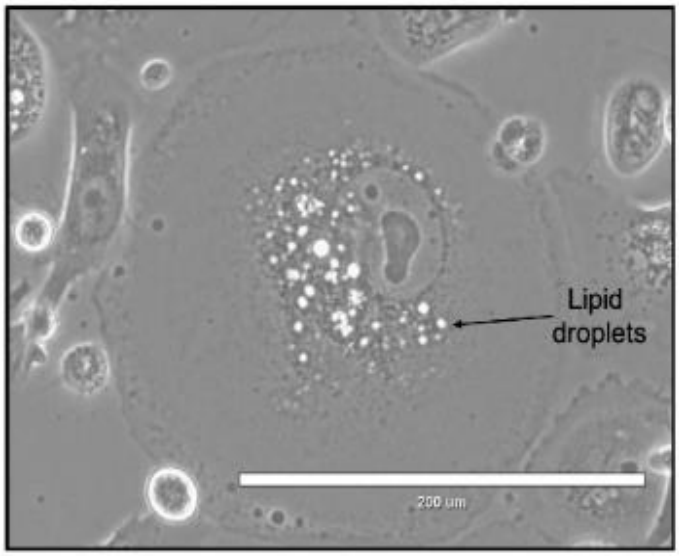

Figure 4: An example of a PACC containing several lipid droplets (black arrow) around the nucleus. The figure is from [21].

What does the cell cycle program of the PACCs look like? Generally, eukaryotic cells undergo a cell cycle comprised of 4 stages – G1 (cell growth; often associated with a related growth phase G0 – resting phase during which the cells are waiting for optimal growth conditions), S (DNA duplication), G2 (preparation for division), M (cell division, or mitosis). A fuller description of the cell cycle and its regulation is available in Section1.4.1. PACCs are typically observed in the

cancer cell culture 72hrs post chemotherapy. The PACCs then are able to persist up until about 10-14 days of exposure to the same treatment during which time they are in G1/G0 phase. It is known that in order to survive a therapeutic insult and go into quiescence, cells go through S and G2 phases, but then they don't proceed through mitosis. Instead, they skip to an endo cycle to go back into G0/G1. As a quiescent state can protect the genome from damages, one speculation is that the PACCs enter quiescence to access the polyploid program and adopt new functions, such as their resistance (Figure 6). After 10-14 days of exposure to the stress, the PACCs are able eventually to re-enter the cell cycle and begin dividing to produce smaller daughter cells that retain the main PACCs properties of resistance and motility.

As the emergence of resistance is a defining feature of PACCs that is connected to their polyploidy, several fundamental models suggest potential paths to achieve this resistance (Figure 5). The first is *the tumor cell heterogeneity model*. Here, the cancer cells already have a mutation present, however, they have to go through the PACCs phenotype cell state transition before they can clonally outgrow. This is not in order to survive stress but to protect their DNA [17].

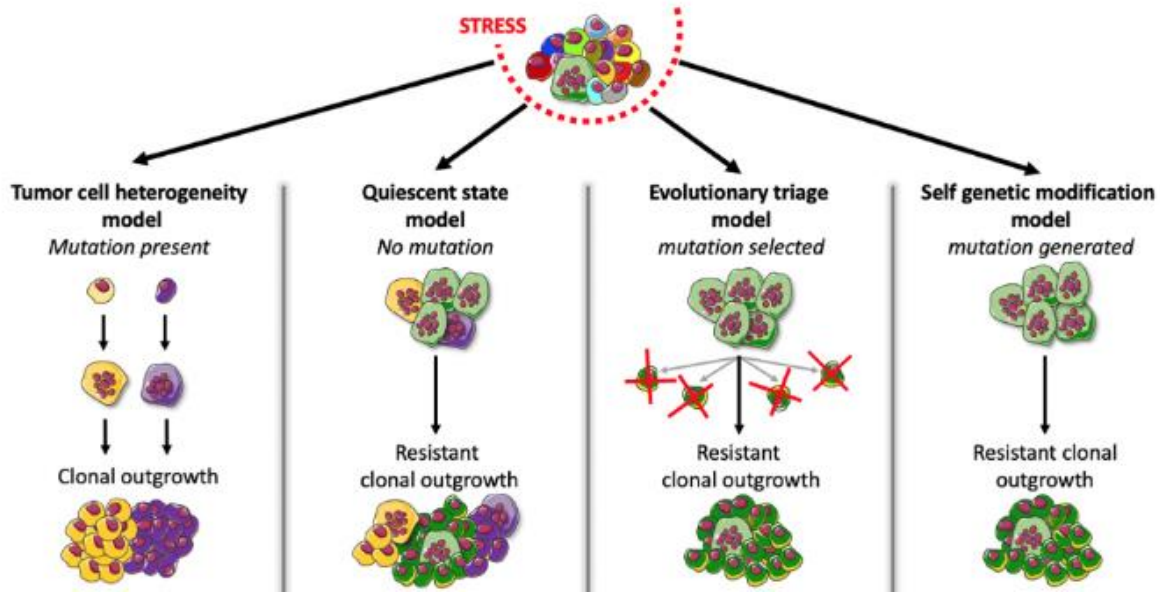

Figure 5: An illustration of the four possible models that make the PACCs resistant. Figure is from [17].

The quiescent state model notes that there is no mutation present before the stress, but rather the original population carries heterogeneous genomes that result in a resistant clonal outgrowth. Another classic model is *the evolutionary triage model* where the extra genomic material is used to spin off variants; most of those will die until the resistant ones outgrow. Finally, there is the idea of stress induced mutation or adaptive mutation that is called the *self genetic modification*

model where cells take time to manufacture a resistant mechanism for a directed rearrangement to generate the resistant clone. Further studies are needed to elucidate an exact resistance evolution model or if there is a combination of several models for different cancer cell lines [17].

Apart from the resistance, the second-striking phenotype of the PACCs is their motility. So far, current studies had been conducted only in 2D *in vitro* environments. Such surfaces, however, are not a common physiological encounter. This raises the question of how will the PACCs respond to an environment that more closely simulates tissue. A full description of the state-of-the-art knowledge on motility and migration can be found in Section 1.4.2. The question relevant to this work is whether PACCs will continue to exhibit motile behavior in 3D and if yes, which type of migration is optimal for such a large cell if it were to exit the primary tumor?

In this master thesis, I have generated PACCs from prostate cancer cells (PC3) through the use of cisplatin chemotherapy and observed them with live-cell imaging in a type I collagen 3D environment in various concentrations.

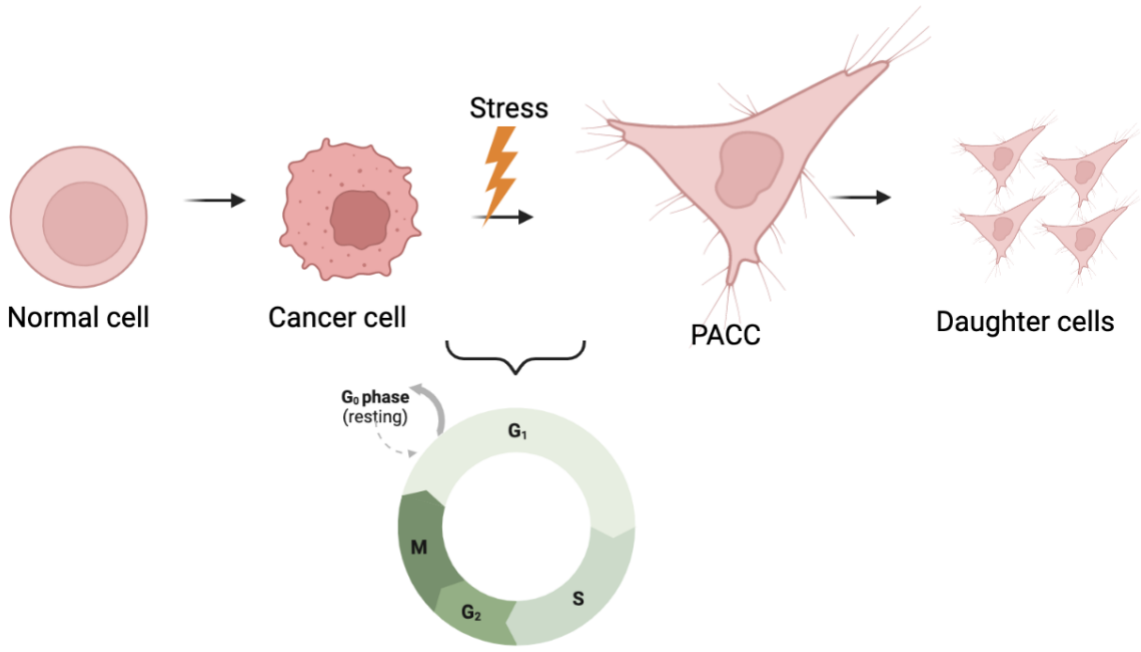

Figure 6: Illustration of the formation of PACCs. From left to right, the normal cell becomes a cancer cell. After experiencing stress, the cancer cell exits the cell cycle program, making it possible to duplicate genetic material without subsequent division. The cell acquires new phenotypes of a significant increase in cell size, resistance to stress and motility. After 10-14 days of exposure to stress, the PACCs produce daughter cells, which are smaller in size, but retain the resistance and motility behaviors. Created with BioRender.com.

1.4 Cell Biology

1.4.1 The Cell cycle

Cell division and the cell cycle were first described in 1882 by Walther Flemming [22]. By using a developing method over time, they were able to distinguish and draw different stages of the cell cycle [23]. The eukaryotic cell cycle includes four phases. The G1 phase marks the beginning of a cell's life and involves cell growth. Some cells may divide very infrequently, but mostly not at all. Some cells can spend a long time in this phase, or the related rest phase called G0, while other more rapidly dividing cell types in adult humans may spend only a few hours in this phase. Then, the cells enter S phase, which takes up to 10-12 hours, and during which the DNA is duplicated and the phase results in two identical copies of the genome [24,25].

When the genome is copied, cells enter G2 phase which is about four to six hours long and causes an incredible amount of cellular activity that must occur in preparation for cell division in M phase. This is because the new cells do not only need their own genome, but also need to produce all other cellular components and organelles. Then, the M phase or mitosis results in the cell dividing into two daughter cells. This phase takes approximately one hour for a mammalian cell. The stage afterward is known as interphase, also called resting time during which there is no division (Figure 7) [24,25].

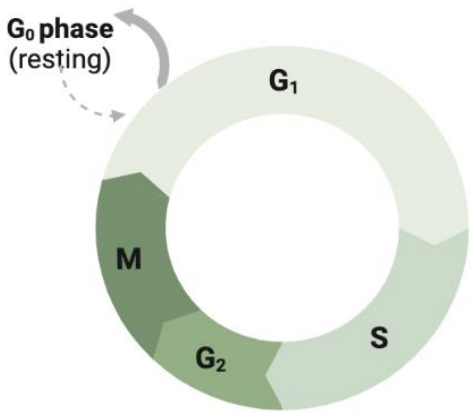

Figure 7: An illustration of the cell cycle. The four phases of the cell cycle are G0, G1, S, G2 and M-phase. The figure is created with BioRender.com.

1.4.1.1 The cell cycle control system

Cell cycle progression occurs by receiving specific signals that cause the exit from one phase and entrance into the next. The regulation of these time-sensitive transitions is performed through a process known as signal transduction. These are molecular pathways transmitting messages within the cell. This particular function is performed by cyclins during the cell cycle, which are small signaling molecules present in the cytoplasm, which bind and trigger the function of protein kinases. The protein kinase is an enzyme that activates or deactivates other proteins by phosphorylation, the act of adding a phosphate group to another molecule. Kinases are typically found in an inactive state and become activated through binding to a cyclin. The bound form of a cyclin and a protein kinase is known as an MPF complex or maturation promotion factors. Unlike kinases, cyclins have varying concentrations in the cell during the progression of the cell cycle with different cyclins being synthesized in each phase of the cell cycle. Through the presence of MPFs and the triggering of activity of kinases, the cell passes the so-called *checkpoints* in order to exit from one part of the cycle and progress to the next. For example, during G1 cells must pass through *the restriction point* in order to be able to progress further through the parts of the cell cycle that prepare the cell for division [25,26,28].

Depending on whether the requirements of the restriction check point are met or not, the cell will either continue to G1 phase or move into G0 which is a non-dividing state.

Most human cells are in G0 phase at any given time; however, they can be called back into the cell cycle. This is done by receiving external signals like growth factors. Another checkpoint is the M phase, and it governs the separation of sister chromatids during mitosis [25,26,27].

Cells are able to exit the cell cycle through naturally occurring processes such as quiescence or senescence. A particularly interesting state is quiescence where cells have exited the cell cycle, but retain proliferative potential and can re-enter the cell cycle and continue dividing, unlike, senescence cells which cannot re-enter [29]. However, cells can also exit or progress through the cell cycle in a deregulated manner, which can result in cells dividing uncontrollably and leads to the development of cancer [26].
Cancer cells do not abide by the signals' instructions that normally regulate the cell cycle. Even in the absence of growth factors or when there is no space for new cells, which are typically indicators to stop dividing, cancer cells may continue to divide. There are numerous causes for this which explains why there are numerous types of cancer, all of which are caused by some

combination of genetic mutations. The immune system may be able to recognize and eliminate a deregulated cell, but if not, it may divide quickly and become a tumor [25,26,28,29].
Therefore, cancer treatment relies heavily on understanding the science behind cell division and cell cycle regulation. Any cancer treatment that hopes to be effective must address the issue on this fundamental biological level.

1.4.2 Cell migration

There is an important distinction to be made when discussing cell movement and that is the distinction between cell motility and cell migration. Cell motility refers to random cell movements, while migration entails movement towards or away from a stimulus [5]. Cells have different ways to exhibit migration. By migration we refer to a cell that is moving towards an attractant (nutrients or another cell) or away from a threat (toxin or a predator). Two types of migration relevant to this study are the amoeboid and mesenchymal types. An example of these two types can be seen in Figure 8 and Figure 9.

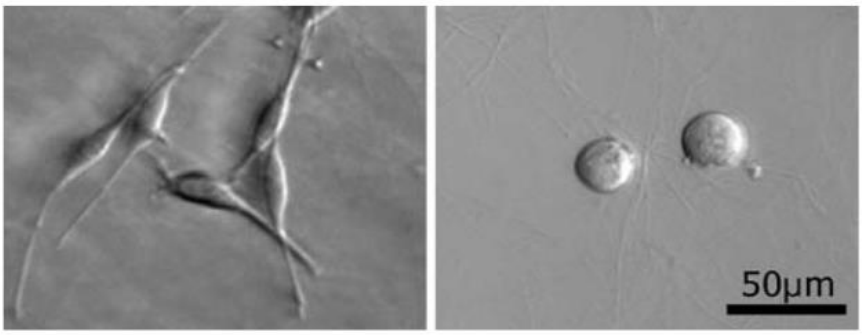

Figure 8: A contrast image of the two types of cell migration recorded during an invasion. The left refers to the mesenchymal shape. The right shows an amoeboid shape. Figure is from [30].

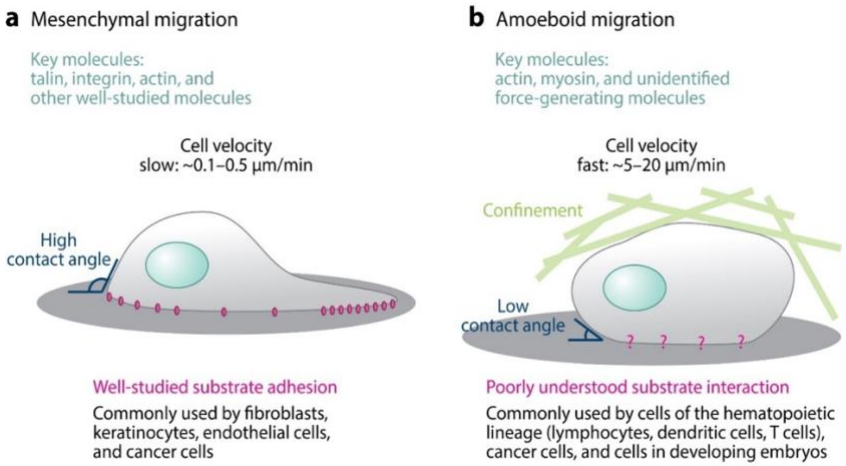

Figure 9: Schematic representation comparing the two modes of migration – mesenchymal and amoeboid. Figure is from [31].

1.4.2.1 Mesenchymal migration

Mesenchymal migration results in cells with an elongated spindle-like shape with their length to width ratio being greater than a factor of two. A cascade of small GTPases is triggered at the preparatory phases of migration that determines the side of the cell where a leading edge will be formed [30]. The cells then recruit their internal actin organization to produce actin-rich filopodia and lamellipodia at the leading edge that allow the cell to protrude forward and begin the process of “crawling” (seen as Stage 1, Figure 10). The protruded part of the cell then needs to adhere to the substrate (Stage 2, Figure 10) at the leading edge, for which further actin polymerization is needed while detaching the back of the cell (or the trailing edge), where actin depolymerization occurs. In these stages the actin-rich structures serve as contractile stress fibers that align with fibers of the extracellular matrix (ECM) through integrin-dependent focal adhesions [33]. The last stage is the motion of the cell body. A contraction from the back will give the cell direction and the cell body motility [32]. The typical cell velocity achieved with this migration mode is approximately 0.1-0.5 μm/min, which is defined as “slow” migration [31].

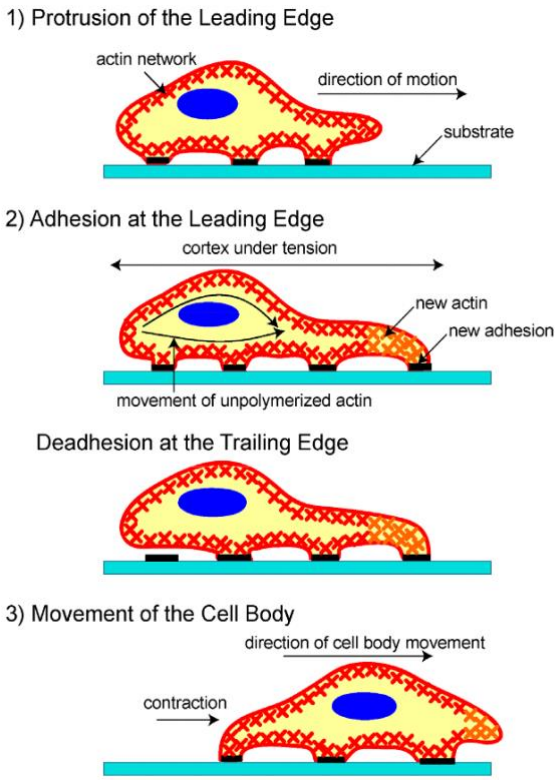

Figure 10: This figure illustrates the process of cell movement. 1) Protrusion of the Leading Edge. 2) Adhesion at the Edge and deadhesion at the Trailing Edge. 3) Movement of the cell body. Figure is from [32].

1.4.2.2 Amoeboid migration

The second type of migration to be discussed in relation to the conducted research project is amoeboid migration (Figure 9). This is a significantly faster migration mode, compared to the mesenchymal migration with cell velocity reaching 5-20 μm/min [31]. This kind of migration shows a rounded and dense cell morphology, with cells often adhering weakly to their substrate. For this reason, this migration mode has been commonly documented in 3D confinements, rather than on 2D surfaces [30]. Generally speaking, the amoeboid type of migration has been less studied, however, recent advances in *in vitro* 3D confinements, coupled with optogenetic approaches have revealed that amoeboid migration can result from plasma membrane flow [34]. Plasma membrane flows are generated through polarization of the processes of endo- and exocytosis at the cell rear and the cell front respectively. This flow of membrane material is coupled to the acto-myosin cortex contractility and the interaction of the two processes is sufficient to propel cells forward [34].

It is imperative to note that cells do not need to exhibit only one type of migration but can switch between the two types when exposed to different environments. The transition often happens at switches from high to low-adhesion, however it also depends on the activity of multiple molecular pathways. In the case of cancer cells this observation is particularly important to keep in mind, as they are exposed to varying microenvironments that need phenotypic adjustments, and such transitions in migration may play a crucial role in metastasis [30,31,32].

1.4.2.3 Chemotactic migration

The current study focuses on the detection of physical stimuli from the environment, such as changes in the stiffness of the presented substratum, however, it is important to highlight the ability of cells to respond to a chemical gradient. The cell migration that occurs in these circumstances is known as chemotaxis. Ultimately, cells do not respond only to a chemical or only to a physical stimulus, but rather to a combination of both. This notion is especially important when we think about what triggers a cancer cell to depart from the original tumor site and what are the indications for arrival and proliferation at a new location. Therefore, considering processes such as chemokinesis, which results in an increase in motility due to the molecular environment [10] should therefore be carefully investigated in future work.

1.5 In vitro studies

In vitro studies allow experimentation outside or apart from a living system and provide a tool to understand the minimal essential components of an *in vivo* process or a system. In *in vitro* experimentation individual components can be introduced in a controlled sequential manner and allow the fine-tuning of individual variables: such as changes in temperature, pH, or physical components such as composition, stiffness, porosity of a substrate. While a great tool to dissect biological topics through a bottom-up approach, *in vitro* work also presents some physiological limitations, as not all elements of the *in vivo* microenvironment can always be introduced and/or studied in a synthetic system [59,60].

1.5.1 3D in vitro studies

To research the migratory and motility behaviors of the PACCs in this project, I created a 3D *in vitro* environment to replicate a tumor-like microenvironment. To achieve this, a 3D encapsulation of the cells in collagen-I type hydrogel was performed and their motility was imaged in real time.

Collagen type I is macromolecule, which helps the integrity of many tissues (Figure 11). The structure of collagen I makes it possible to produce collagen matrices to mimic an *in vivo* environment. As collagen is derived from living organisms, it provides an opportunity to compare the results of the study to a closer *in vivo* situation [60,61].

Figure 11: An illustration of type 1 collagen, which is a straight triple helix. Figure is created with BioRender.com.

However, the polymerization of collagen in different concentrations can result in different collagen matrices. Increasing the collagen concentration results in an increase of the elastic modulus of the produced hydrogel [62]. The opportunity to fine tune the collagen concentration can allow for a match to be made between the produced stiffness of the hydrogel and for instance, a living tissue. The stiffness of a hydrogel can be defined by a physical property, such as the Young's modulus, by utilizing for instance optical tweezer experimentation [48,63].

Figure 12 provides a view of how the collagen matrix would look like depending on the concentration.

Figure 12: An illustration of collagen matrix in increasing concentration. Figure is created with BioRender.com.

2 Material and Methods

2.1 Materials

For the generation of PACCs, the following item list was used: pluriSelect filters, 15 µm pluriStrainer Cell Strainer (pluriSelect REF:43-50015-01), pluriSelect Connector Ring (pluriSelect REF:41-50000-01), T-75 flasks, 50 mL conical tubes. For imaging: 96-well transparent flat-bottom plates (Corning).

2.1.1 Solutions and reagents

Complete medium composition: DMEM (Gibco), 10% FBS (Gibco), 1x ZellShield (Minerva Biolabs). For cell line propagation and generation of PACCs additionally used: sterile 1x PBS (Gibco), sterile TryplE-EDTA 0.05% (Gibco), filter sterilized Cisplatin (3mM), used in final concentration of 3 µM (kind gift from Prof. Dr. Emma Hammarlund lab, University of Lund). For the collagen gel preparation: Collagen type I rat-tail, FirstLink, MEM 1x (Gibco), NaOH (SigmaAlrdich).

2.1.2 Equipment

Nikon Eclipse Ti-E microscope, with incubation chamber – 37°C, 5% CO_2, 20x objective. Cell counter Life Technologies.

2.1.3 Maintenance of cell lines and cell culture

The PC3 cell line was received as a kind gift through the collaboration with Prof. Dr. Emma Hammarlund lab from University of Lund. The cell lines were kept in the -80 ℃ freezer. The cell line was maintained and propagated using standard protocols [35].

2.2 Protocol for PACCs generation

The protocol extends over 10 days.

Seeding: (day 1)

The original cancer cell line, PC3, was seeded for a final cell concentration of $1x10^6$ cells in a T-75 flask. The control cells that are not to receive treatment were also seeded on the same day in lower concentrations (about 250.000 cells). Cells are then placed in a 37°C incubator, 5% CO_2 for 24 hours.

Treatment: (day 2)

The complete medium is removed, the cells are carefully washed with 1x PBS, and treated with a drug master mix (medium+antibiotic, f.c. 3 µM cisplatin) into the same T-75 flask. The cells are left with the drug mix in the incubator for 72 hours, which yields the largest quantity of PACCs. Typically, for a treatment with cisplatin of IC50 of 6 µM, the expected yield from 1million seeded cells is ~250.000 to 300.000 PACCs (Figure 13).

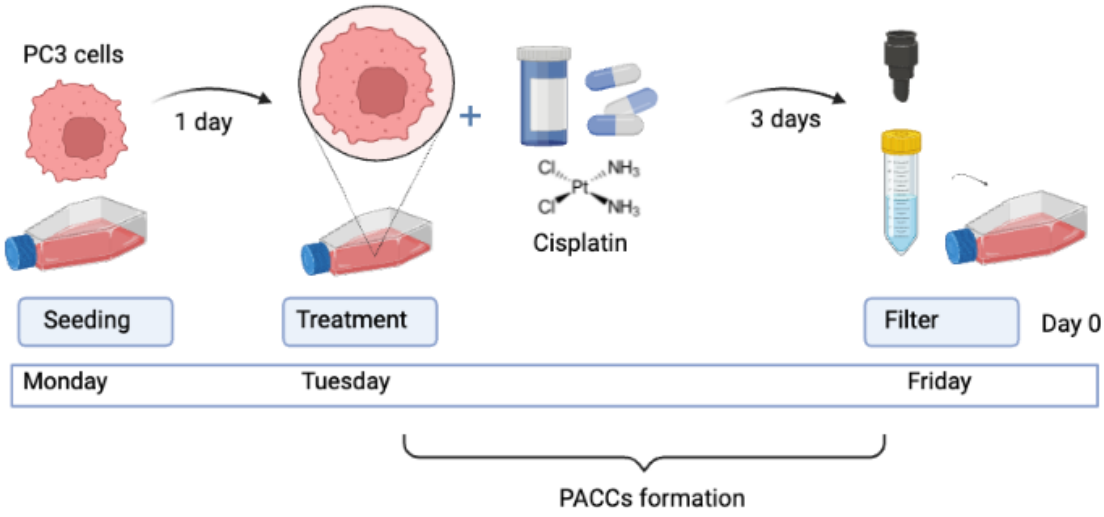

Figure 13: Part 1: An illustration of the formation of PACCs protocol (week 1). In the first week pre-treated PC3 cells are seeded and receive treatment the day after. The treatment is chemotherapy with 3 µM Cisplatin. Three days post-treatment, the formation of PACCs has occurred and the PACCs have to be filtered away from sister cells and dead cells. Illustration created with BioRender.com.

Filtration: (day 5)

On day 5 the PACCs are formed. This is appreciable by light microscopy (Figure 14). However, the PACCs are accompanied in the flask by cell debris as well as sister cells. Sister cells are cancer cells that remained resistant to the treatment but have not converted to PACCs and therefore have retained a cell size similar to the original cell line. These cells were not a part of the investigation that pertains to this study. Therefore, the PACCs were filtered.

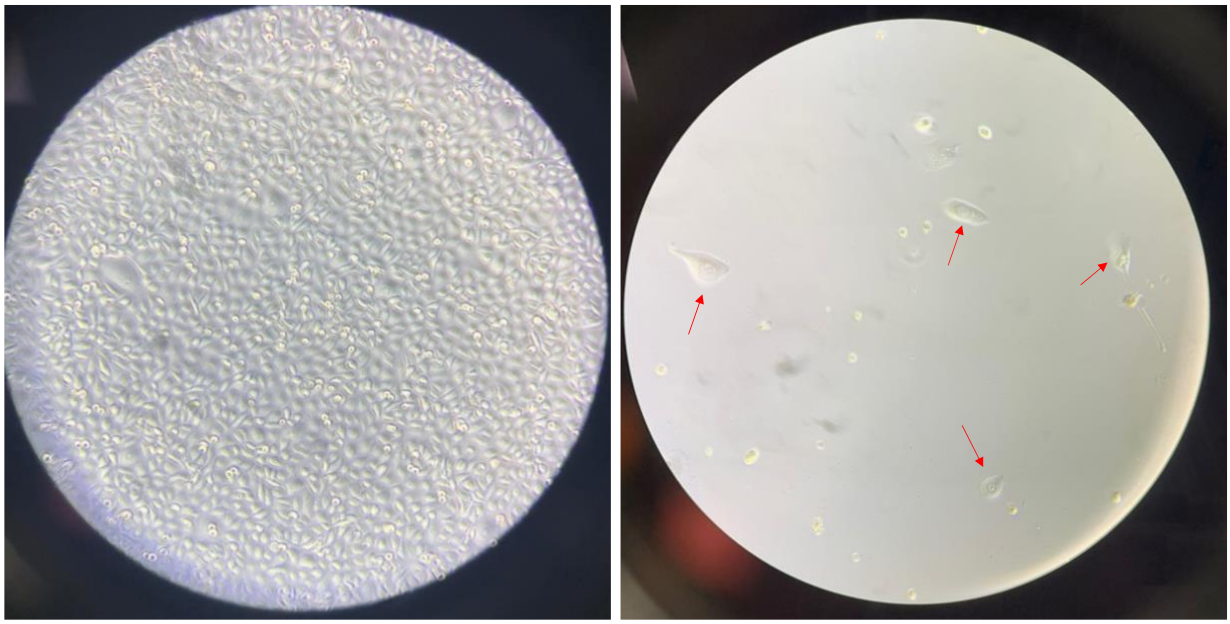

Figure 14: Left image, non-treated PC3 cells at 100% confluence. Right image; PC3 cells and PACCs (four red arrows) after the treatment. 10x Bright Field microscopy, Leica light microscope.

The process for filtering the PACCs starts by gently washing the cells with 1x PBS. Cells are lifted with TryplE similarly to the cell seeding, however, cells resuspension is 20 mL complete medium in a 50 mL Eppendorf tube. The more diluted the cells are, the less likely it is that they will experience filter clogging. Two connector rings with filters are placed on two 50 mL conical tube. It is recommended to use 2 filters per 1 T-75 flask, as too many cells will cause excessive filter clogging. First, 5mL of complete medium will be gently added on top of the filter for priming the filter. As the media will usually not flow through the filter immediately, pull the media through with an aspirator on the lowest suction force connected to the connector ring to pull the media. Preferably to not use the aspirator for the following steps of the protocol if it can be avoided.

Slowly pipette 5 mL at a time the cell suspension on top of the filter.
Most of the suspension will flow through on its own. However, at the end, some clogging may occur that prevents steady flow through. If this occurs, then the aspirator can be used to gently aspirate at the lowest suction force, pull the rest of the sample through the filter. Once all cells have been filtered, the filter will be removed and placed the one-at-a-time upside-down into a new 50 mL conical tube. Last, each filter will be washed with 10 mL complete medium. For this part it is important to be forceful, which means to press the pipette directly against the filter. It is also important to be sure to cover all areas of the filter, so as to collect as many cells as possible.

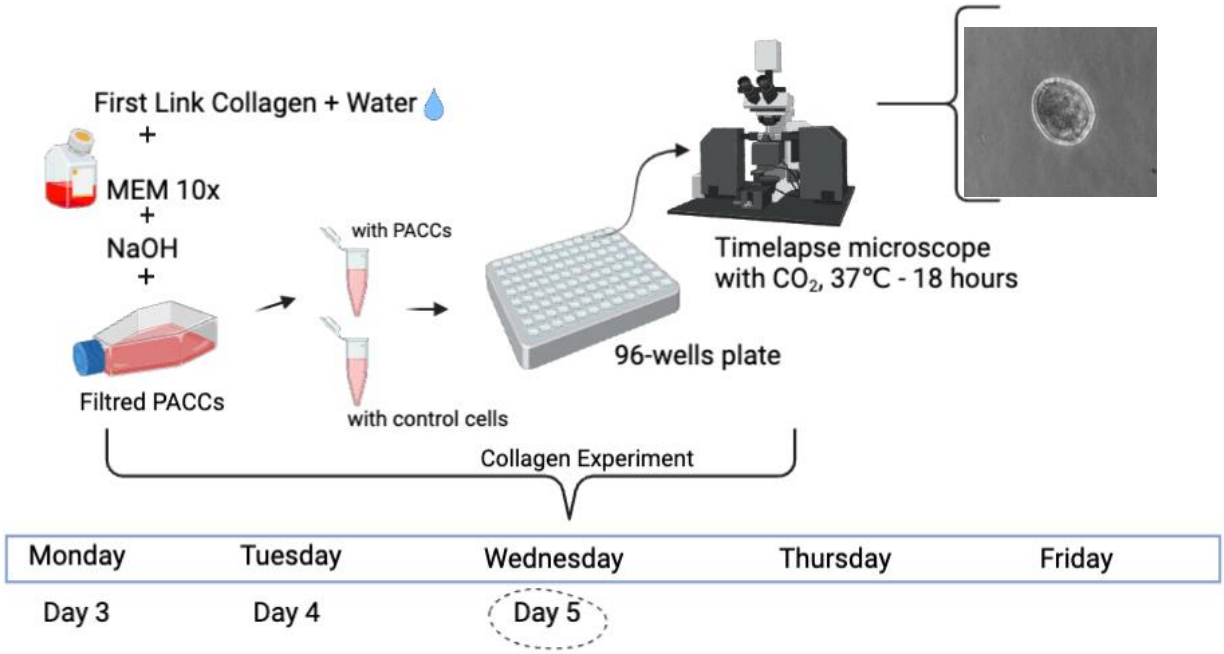

Figure 15: Part 2: An illustration of PACCs collagen encapsulation (week 2). After keeping the filtered cells for five days after the filtration, the collagen experiment will take place. Combining First Link collagen (type I), H_2o, MEM 10x, NaOH and the cells, a 3D environment is provided for the cell encapsulation. Two separate samples are prepared, one with PACCs and another with control cells for comparison of the two cell types. 96-well plates are used by adding ~200 µl of the collagen mix with cells per well. After leaving the 96-well plate (as is in the figure) in the incubator for ~30 min, the cells will be imaged in real time with the Nikon Ti-Eclipse microscope for ~18 hours every 10 min On the right side an example image from the microscope. Illustration created with BioRender.com.

After the filtration, PACCs are counted. Centrifugation of the filtered collected PACCs, 5 min at 1000 RPM. The supernatant is aspirated and the pellet of PACCs is resuspended in 1 mL complete medium for standard protocol of cell counting. One should expect a low cell count number, ~250.000 – 300.000 PACCs per each T-75 seeded on day 1. Importantly, the cell counting for PACCs will not be precise as for other cell types, due to the large cell size of the PACCs. Typically, the counter displays a value of at least 2x higher cell count than the real number of cells in the suspension. Through empirical evidence, I can conclude that the number can be overestimated even up to 3x. This is highly important when considering the number of cells to be distributed for later imaging in each well of a 96-well plate.

The PACCs are then provided with fresh medium without antibiotics and returned to the incubator, 37°C, 5% CO_2. The PACCs from the day of filtration are indicated as Day 0 PACCs. On day 5 the collagen experiment will take place. Figure 14 shows an example image from the light microscope of PACCs on day 5.

2.3 Simplified protocol for collagen samples preparation

Full description of the protocol and its optimization is in the section below, "*Collagen experiment preparation*".

Procedure:

- Remove current media.
- Wash the cells with PBS and lift them with Trypsin.
- Spin them down with the centrifuge for 5 min at 125 RCF.
- Aspirate the medium.
- Resuspend the pellet in 1 mL complete media.
- Count the cells. Calculate for a cell count of 7000 cells per well in a 100 µl cell suspension in 1 mL total volume of collagen mix. The cells are resuspended with complete media.
- The mixing should be done on ice. Keep the NaOH, MEM and collagen cold by putting 1 mL in a cold Eppendorf tube on ice. The cell suspension should not be on ice.
- Follow this order during the mixing: (Total volume 1mL, full recipes in Section *Collagen experiment optimization*)
    1. MEM
    2. Collagen
    3. NaOH
    4. Cell suspension
- Dispense 200 µl from the 1 mL collagen mix per well
- Put it in the incubator for around 30-40 min
- Add 100 µl complete media on top of the collagen.

Note: Remember to pipette slowly and to use cold pipettes to decrease making bubbles

Note: For a low concentration of PACCs, spin them down again, 3 min at 125 RCF.

2.3 Experiments

2.3.1 Collagen experiment optimization

Different concentrations of collagen were tested to identify an optimal environment where the cancer cells can survive as well as display motility in the gel. 2, 1, and 0.5 mg/mL collagen concentrations were used for the final experiments.

Additionally, a wide range of cell concentrations per well were tested in order to optimize the later imaging. The goal was to have at least 1 to 5 cells per field of view. Since the PACCs and control cells have different cell sizes, this amounts to a different number of cells per well. For both cell types, I tested a range of cell concentrations from 500 to 7000 cells per well. Ultimately, 7000 cells per well were used for PACCs and 5000 cells per well were used for the control cells. Importantly, the PACCs were provided with both conditions: present alone in a field of view with no neighbors (in several 2 mg/mL collagen) and present with at least 1-3 neighbors (in the remaining experiments).

Given that the collagen experiment is prepared in cold conditions, some key optimizations are the cooling of all equipment and optimizing a fast-pipetting order. At the same time, pipetting must be as gentle as possible to prevent bubble formations, which are harder to avoid at the beginning of the polymerization process in cold conditions.

For the preparation of a 2 mg Collagen, the following mixing order was optimized and carried out for all experiments: 100 µl MEM 10x, containing phenol red pH indicator, is mixed with 800 µl collagen. Approximately 80 µl NaOH is added to neutralize the solution from acidic to neutral. The pH change was indicated by the final color shift from bright yellow to soft pink. The cell suspension is mixed into the above-mentioned solution. Subsequently, 200 µl of the final collagen mixture was added per well. The same procedure was repeated for the control cells. Afterwards the 96-well plate was placed in the incubator with CO_2 and 37°C for around 30-40 min. 100 µl complete medium (with FBS and Zellshield) were then added on top of the collagen mix. The amount of additive material for the 2 mg/mL, 1 mg/mL, and 0.5 mg/mL collagen can be seen in Table 1.

Table 1: 0.5 mg/mL, 1 mg/mL and 2 mg/mL collagen concentration preparations used for this study.

Collagen concentration	Recipe:
0.5 mg/mL	100 µl MEM 200 µl Collagen 580 µl H20 20 µl NaOH 100 µl cell suspension
1 mg/mL	100 µl MEM 400 µl Collagen 360 µl H20 35-40 µl NaOH 100 µl cell suspension
2 mg/mL	100 µl MEM 800 µl Collagen 70-80 µl NaOH 100 µl cell suspension

2.4 Time-lapse imaging

The Nikon Eclipse Ti-E microscope was used as the imaging system for this study. The microscope has an incubation box connected with a heater and CO_2. This helps ensure that the conditions are as similar to the incubator conditions as possible. Temperature was set to ~37 ℃ and CO_2 5%. Throughout the duration of the study, another microscope was also tested, the Juli Stage Real-Time cell history recorder (NanoEntek), which can image directly inside of the incubator. However, due to technical difficulties with the stage automation, the microscope was not available for reliable data collection. Therefore, the Time Lapse microscope was utilized, even though the conditions inside of an incubation box attached to a microscope are not as stable and ideal for cell growth over the 18 hours imaging period. To improve the conditions, the stage is located inside a black plexiglass box that ensures a closed system with controlled heat and CO_2. Nonetheless, there were clearly conditions in which cell growth, and cell division were observed throughout the entire imaging period, suggesting that the cells were in a sufficiently favorable environment. This confirmed the use of the Nikon Time Lapse. A 20x objective and brightfield, has been used during all experiments.

Multipoint acquisition was performed every 10 min for 18 hours, resulting in movies with 109 frames of the cells in brightfield. The images acquired were 2160x2560 pixels and the pixel size were 0.33 µm/px. (Figure 15).

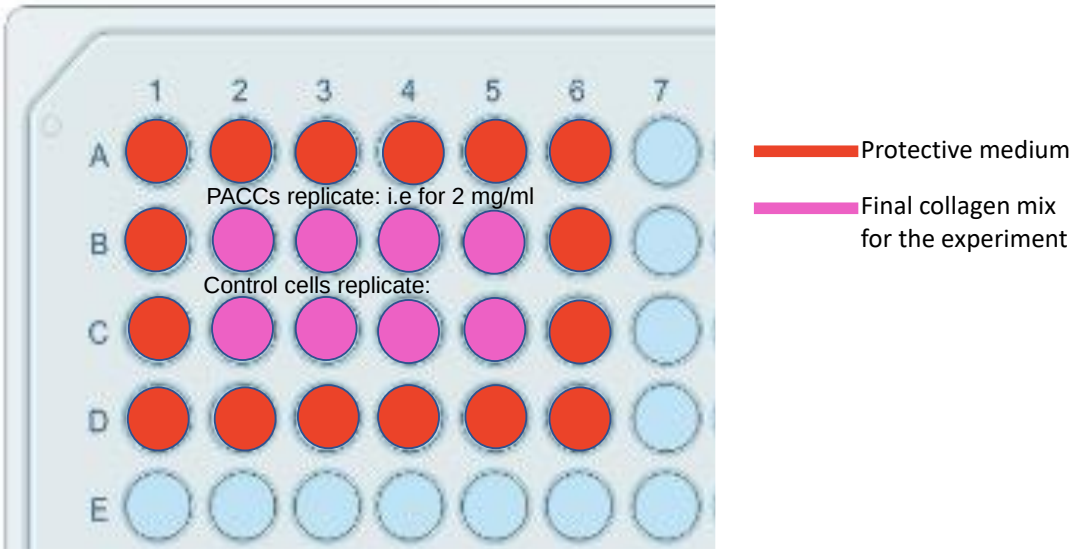

Figure 16: An illustration of the 96-well plate used to image the cells in the 3D environment with PACCs (row B2-B5) and control cells (row C2-C5). The final collagen mix is surrounded by the protective medium. The illustration of the 96-well plate is created with BioRender.com.

2.5 Imaging analysis

The purpose of the image analysis is to end up with tracks from cells which have been recorded on the microscope. We will get individual tracking of the cells, which will give the coordinate for their center of mass positions [x(t), y(t)]. This will be relevant as we want to analyze the motion of the PACCs and the control cells.

2.5.1 Image preprocessing

For the pre-processing, we started by opening the .nd2 files from the microscope in FIJI to crop the video to a smaller file size, as the file otherwise will be too big for the software to process As the software, Interactive learning and segmentation toolkit (Ilastik) [42] read files either in HdH5 files or .tiff, the original raw data movie was saved as .tiff from FIJI. As another software is used for the cell tracking, called TrackMate plugin in Fiji, and the plugin works best with pre-processed images this was an important conversion. As the images are taken in brightfield, it can be difficult for TrackMate to distinguish between the background and the cell (Figure 17).

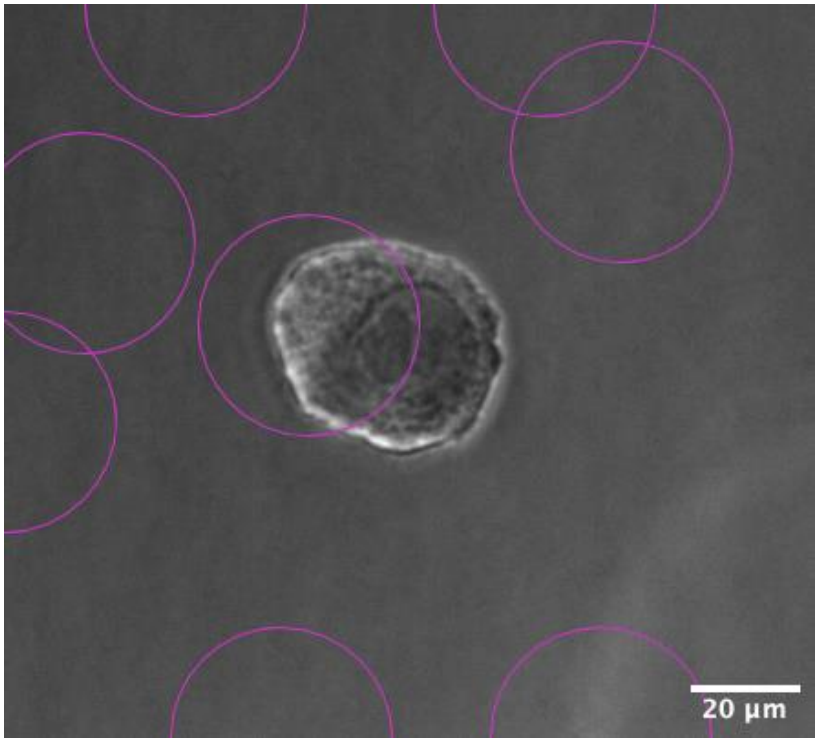

Figure 17: The brightfield image without any Pre-processing shows that using the plugin TrackMate directly we cannot identify and segment the cell correctly.

2.5.2 Ilastik

Ilastik is a machine learning software to classify images [42]. It has the advantages to distinguish between different intensities of pixels. This property allows labeling the target of the investigation. In this case, we want to label the cells and the background.

To perform the segmentation of an image, *Pixel Classification and Object Classification projects* were selected. The combination of the two properties means, first and foremost, it can select the category it belongs to using the pixel intensity. In our case, we are interested in classifying the cells and the background. During this research project, the software could not necessarily segment or recognize all the cells. For example, the data was pre-prepared by identifying manually and eliminating dead cells. In such cases, manual segmentation was performed. This was done using a brush function, where one could mark the cell or the background by hand. The background was also sometimes manually adjusted, as the brightfield image could have some blurred backgrounds, which Ilastik could detect as cells. All in all, adjustments were made so that the processed images would match the original ones. In addition, there was another feature called object classification which helped make the previous segmentations from pixel classification into objects.

Furthermore, objects that had a pixel value corresponding to the cell or background were divided (Figure 18). This feature was also an advantage for pixel values placed under the cell category, even if it was not under that label, could be edited, so the not-label cell could be label. This was done at the threshold size ratio. This threshold ratio helps edit and, among other things, reject small stuff, which is not the cell, like in Figure 18 to the right. Nevertheless, some of the cells were not always corrected, as some of them, such as the control cells, were dividing. This resulted in the program not registering the segmentation. This is also partly due to the fact that there is a low contrast in the original images that comes from the microscope. Another example that indicating potential software issues is about for cells with long filopodia arms. In this case the software would detect two cells instead of one. Therefore, this was also checked as thoroughly as possible during the TrackMate Fiji plugin use. TrackMate can manually track the cells if something does not match with the original images.

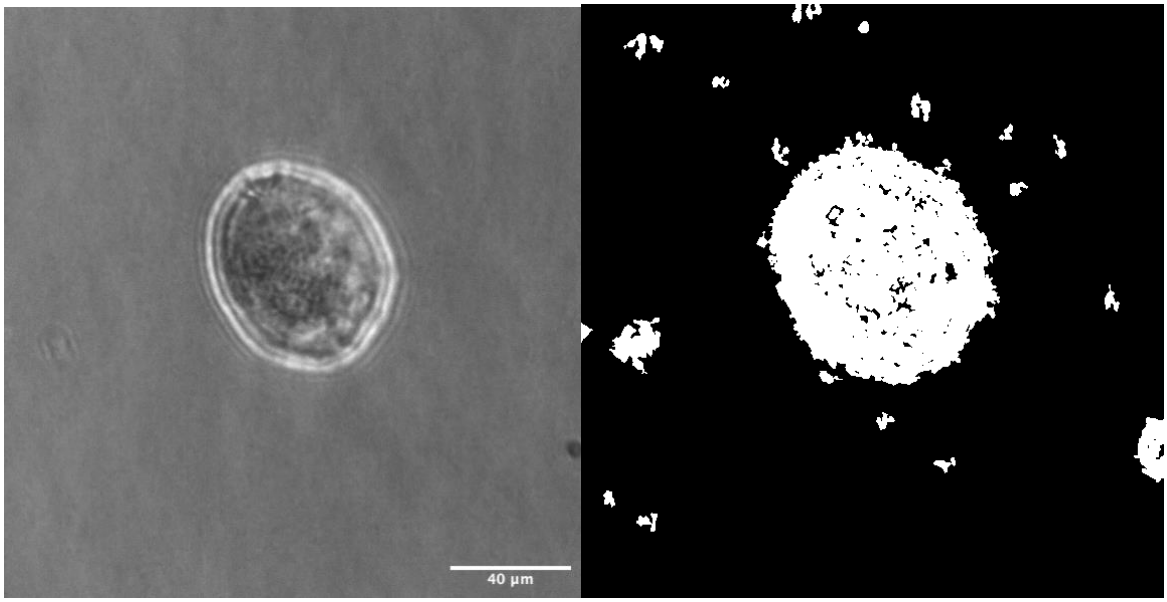

Figure 18: The transformation of microscope image through the Ilastik software. Left image: the brightfield image of a PACC without any preprocessing. Right image: Ilastik processed image.

A template was made for the control cells and the PACCs. By having a template, it was possible to run more than one file at a time. One file in this case means an individual frame of the movie. One dataset can contain up to 17 frames (a series) that includes the control cells and the PACCs. This was a huge advantage to reduce the processing time. On the other hand, there is the disadvantage that running more than one file could take more than 12 hours, making the processing of one dataset with one to nine files for controls and PACCs take more than 24 hours.

Ilastic presents some limitations and is in need of a few manual adjustments, however overall it is a useful tool that I familiarized myself with for the purpose of this study, but have also taken advantage of how other have been using it for the same purpose in the literature [36,37].

Figure 19: Another example of the final result using Ilastik, namely the binary image of a PACC, which were used end the end to track with TrackMate from Fiji.

The result of the program will be a binary image where we have segmented the cell and the background, which will make it easier to track the cells with TrackMate (Figure 19).

2.5.3 Single cell migration/tracks: TrackMate plugin in Fiji

After all the cells were run through in the ilastik, they were now ready to be tracked with TrackMate in Fiji. TrackMate provides a tool to track individual tracks [43]. In addition, TrackMate also has the property to manually detect the number of existing spots. Depending on the cell size, an estimated cell size was given. A detector was then selected. In this case it was the *Downsample log detector*. This is due to previous reporter who have investigated the same in relation to the purpose [36]. Additionally, a *threshold* of 0.45 was chosen. For the *initial thresholding* all was selected. *The selected view* was selected to *be Hyperstack Displayer* and all *set filters on spot* were selected too. The algorithm was chosen to be the *simple LAP tracker*,

including linking max distance (50 μm), gap closing distance (50 μm) and max frame gap (5). *Duration of tracks* was selected as filter on tracks. Last, the tracks were edited manually with *TrackScheme*. The aim of the cell tracking is to find the coordinate of the center of mass to further investigate the cell's motion across the field of view. For detailed performance of TrackMate previously reports were used [36,37].

Some rules were considered to establish which cells were tracked or not tracked. One of the rules for the cells to be tracked in the first place was that the cell had to be defined as “alive”; to stop following the tracking of a cell which has divided, and to instead divide the new tracks over the two new daughter cells. This was performed manually as TrackMate had trouble detecting the appearance of a new cell. Instead, its misrepresented the data as if the original cell was experiencing a long motion. Originally, this led to incorrect tracks, which were subsequently corrected.

2.6 Data Analysis

2.6.1 Data preprocessing

Since the tracking of cells starts at different positions and times, some preprocessing is needed before the experimental trajectories can be used for further data analysis. First, the software recorded the evolution of the tracks as number of frames, therefore, this magnitude had to be converted to units of time, minutes particularly. The position of the cells also needed to be converted to physical units, in this case from pixels to micrometers. The metadata of the experimental files provided the information to perform the change of the units as the images acquired were 2560x2160 pixels and the pixel size was 0.33 μm/pixel. Once the data is converted to the appropriate units, all the tracks are transposed so they present the same starting point in space and time.

$$\begin{aligned} T(i) &= t(i) - t(0)\ for\ i = 0\ to\ N \\ X(i) &= x(i) - x(0)\ for\ i = 0\ to\ N \\ Y(i) &= y(i) - y(0)\ for\ i = 0\ to\ N \end{aligned} \tag{1}$$

, where N is the total number of measurements per track.

2.6.2 Displacement analysis

The Brownian motion is a well-known stochastic phenomenon discovered by Einstein in 1905 [38]. A particle following a Brownian motion from time zero can be described with the distribution:

$$P(r,t) = \frac{1}{\sqrt{4\pi Dt}}\, e^{\left(\frac{-r^2}{4Dt}\right)}, \tag{2}$$

where *t* is the time, *r* is the distance and D is the diffusion constant.

Mean squared displacement (MSD) calculates how far a particle or cells move over time. It is used to characterize random trajectories and used to see how a particle deviates from an initial point. In biophysics is used to determine whether a particle Is spreading slowly due to diffusion, i.e following a Brownian motion, or if and advective force is also contributing to the movement [38]. The MSD of an ensemble of cells is:

$$MSD \equiv < |r(\tau) - r(0)|^2 > = \frac{1}{N}\sum_{n=1}^{N} |r^{(n)}(\tau) - r^{(n)}(0)|^2 \tag{3}$$

where <> is the ensemble average (EA), $r^{(n)}(\tau)$ is the position of the n*th* cell after time, $r^{(n)}(0)$ is the starting position of the n*th* cell pathway. Last, N is the total number of cells considered in the ensemble.

The particles in biophysical systems may follow more complex types of migration, aside from the Brownian motion. These different movements can be close to a diffusion process or be completely different to it.

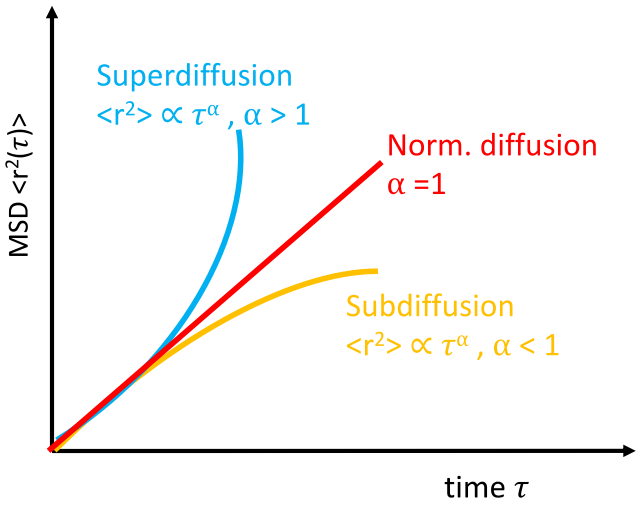

Figure 20: Visualization of the different regimes of diffusion for different anomalous coefficients. Red line) shows the behavior of a Brownian motion, blue line) shows the superdiffusion regime, and yellow) represents the subdiffusion regime. Figure is modified from [37].

In order to describe these more complex trajectories the MSD can be formulated as a power law. This MSD expression presents the anomalous coefficient, whose value allows to find if a particle follows any of the different diffusion regimes:

$$< r^2(\tau) >= K_\alpha \tau^\alpha \tag{4}$$

, where α is the anomalous coefficient and K_α also known as the generalized diffusion coefficient [64]. Depending on how the curve of the MSD looks the value of α will change. Equation 4 has been used in this study to determine how the motion of our cells differed from a diffusive movement [38,39,40]. The different values that the anomalous coefficient can present represented in Figure 20 are:

- $\alpha < 1$ the trajectory is comparable to a *subdiffusive* movement. The MSD value starts decreasing as time advances as seen in Figure 20, yellow line. This can indicate that the motion of a particle is non-active as it moves slower than a Brownian motion.

- $\alpha = 1$ the movement is comparable to *Brownian motion*: By Brownian motion it means that the movement of the particles could be replicated with a random walk.

- $1 < \alpha < 2$ the trajectory is comparable to a *superdiffusion* movement. Here the MSD grows more compared to the other lines. This could mean that particles have a more active motion in the beginning of a process.

- α = 2: the trajectory is comparable to a *ballistics motion*. By this it means that the particles are accomplished with a high velocity and acceleration.

So, in Figure 20, the different behaviors previously explained can be visualized. MSD is an important tool which can be used to identify the type of anomalous diffusion processes. Last, Anomalous diffusion has been observed in many different fields in physics. By using it is possible to find the way the particle or cell is diffused [37, 39, 40].

2.6.3 Trajectory quantification

The trajectory of the particles can also be studied with other quantities apart from the MSD.
In this study we use the end-to-end length (r_{ee}) to gain more information about our system.
The end-to-end length (r_{ee}) is defined as the position of the first point to the final position of the end point (eq. 5):

$$r_{ee} = |r(t_{end}) - r(t_0)|, \tag{5}$$

Where t_{end} is the last time point of the track. So, a big r_{ee} distances mean that the particle has moved from its original point following a preferred direction of motion.

2.7 Statistical analysis

There are various approaches to define a typical value from a set of N elements of data, but the mean value is defined as:

$$\mu = \frac{1}{N}\sum_i x_i \tag{6}$$

Once the mean value of the data set is known the standard deviation, (σ), can be computed as:

$$\sigma = \sqrt{\frac{1}{N-1}\sum_i (x_i - \mu)^2} \tag{7}$$

, where σ is the standard deviation (SD) of the data set.
Different data sets can be compared to see if their samples come from the same distribution. In this study we compared pair of datasets. The first thing we did was to find if the data sets followed a normal distribution. If the two quantities to be compared were normal we used a T-student test [65]. In a T-test the average values of the two data sets are used to determine whether they come from the same population. In a similar way the Mann-Whitney U-test is a non-parametric statistical test that tells us if the two data sets come from the same population when they do not follow a normal distribution [66].

When performing a statistical test we obtain a p-value. The p-value can be compared to a typical significance level, α, and it represents the probability of observation under the null hypothesis. In this study the significance is set to $\alpha = 0.05$. The null hypothesis is false if the p-value is less than α and the distributions are statistically different [67].

2 Results

In vitro studies and cell imaging:

Upon the generation of PACCs from prostate cancer cells (PC3), the cells are left in culture for five days. The 5-day mark was selected as previous work demonstrates that PACCs typically develop motility on 2D surfaces at that time point (Figure 22). The selection of this time point was paramount, because the experiment calls for harvesting the highest number of alive motile PACCs, which was estimated to be on Day 5 post-treatment. At that time, on a 2D surface, a PACC moves via mesenchymal migration (see Figure 22). Once visually confirmed by microscopy that the majority of surviving cells post treatment were indeed motile PACCs, those cells were lifted from cell culture and introduced in a 3D collagen gel (type I) in three concentrations. The used collagen concentrations were 2 mg/ mL, 1 mg/ mL, and 0.5 mg/mL. These concentrations were selected based on literature suggesting that the 2 mg/mL concentration of this specific brand of collagen (FirstLink) was optimal for cell encapsulation [44,45,46,47,56]. The exact same concentration and brand of collagen was also used in a study investigating the encapsulation of motile cancer cells to study their invasion and colonization abilities [49]. More details on the procedure and a schematic depicting the process can be found in Materials and Methods Section.

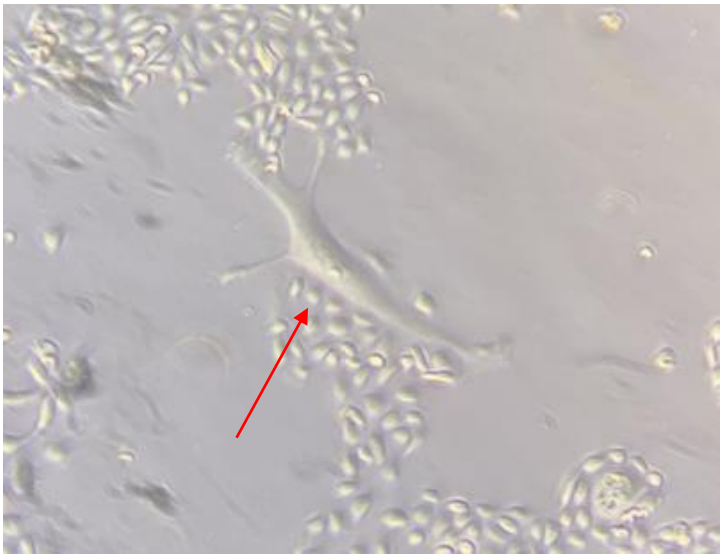

Figure 22: A PC3 PACC (red arrow) on a 2D surface. The image is taken from the light microscope by mobile phone camera. The PACC moves via mesenchymal migration.

Here, it is important to note that encapsulation of living cells and their imaging is a non-trivial process, which involved several optimization steps, such as:

- Optimization of the collagen gel preparation and polymerization.
- Cell preparation and optimization of the use of exact cell concentrations.
- Cell embedding in the gel to ensure cell survival over the imaging period.
- Selection of optimal microscopy set-up allowing the continued unperturbed visualization of the cells.
- Selection of the optimal imaging time-frame and duration.

Details on these optimization steps are presented in the Material and Methods section.

Due to the presence of motility of PACCs on 2D surfaces, a hypothesis was formulated that a 3D environment, which is more similar to the physiological environment of tissue, could trigger either a more engaged form of migration or a different type of migration, compared to the one observed in 2D.

I performed the following set of experiments presented below in order to test this hypothesis

Real-time imaging provided the opportunity to investigate the PACCs and compare them to the pre-treated PC3 cells when both are encapsulated in a 3D environment. Microscopy was performed every 10 min for 18 hours using a Timelapse brightfield microscope with a 20x objective, monitoring growth conditions (CO_2 and temperature, 37 ℃) The duration of 18 hours was selected, since it was observed that sometimes the PACCs did not exhibit any major migration behaviors up until 14 hours.

The advantage of using brightfield microscopy is that it is an approachable non-laborious method that provides a non-invasive environment for the cells. Complications such as photo-toxicity can be avoided, and the cells can be observed in an as close to a natural state as possible. The following parameters were of particular interest: cell motility, cell death, and cell division. All of these parameters could be potentially altered if the cells are expressing additional fluorescently tagged proteins and/or are subjected to intense light for the prolonged period of time for which observation was needed (18 hours).

This experiment structure allowed the collection of varied qualitative and quantitative data. Analysis of each individual real-time imaging movie allowed for a detailed overview of the data by separating it in categories. Firstly, it was important to report on the proportion of cell death: do both cell types – untreated cell line PC3 and their PACCs - survive the encapsulation of the

three different collagen concentrations? Second, does the encapsulation still provide beneficial enough environment where the cells can cycle through their cell cycle and undergo division? And lastly, whether the cells exhibit any movement. Cell death and cell division are quantitatively described, while motility, which is a complex cell phenotype is described in both qualitative categories and through quantification of cell tracks.

3.1 Quantification of cell survival during encapsulation

Figure 23 shows the number of dead and living cells per cell type in each collagen concentration. Cells were categorized as “dead” based on either being already dead in the first place or that they died in the duration of the experiment. This can be seen in figure 24B and 24C (the one below, in brightfield) Comparing the results from PACCs versus control clearly shows that PACCs experienced more cell death events. For the control cells in 0.5 and 1 mg/mL condition no cell death was observed, while in 0.5 mg/mL 45 PACCs were counted, out of which 17 cell death occurred for the PACCs in the same collagen concentration. In 2 mg/mL of collagen concentration, the PACCs show an even higher cell death compared to 0.5 mg/mL and 1 mg/mL conditions with more than 50% of the PACCs dying. At the same time, the 2 mg/mL condition also affected the control cells where now cell death can be reported (9 cells). These data are indicative that the 0.5 mg/mL and 1 mg/mL conditions provide a more stable environment where cell death is less likely to occur and therefore could be considered closer to a physiological-like environment. A publication from Wullkopf. et al, 2018, [48] shows that the 1 mg/mL collagen condition has similar stiffness to human tissue.

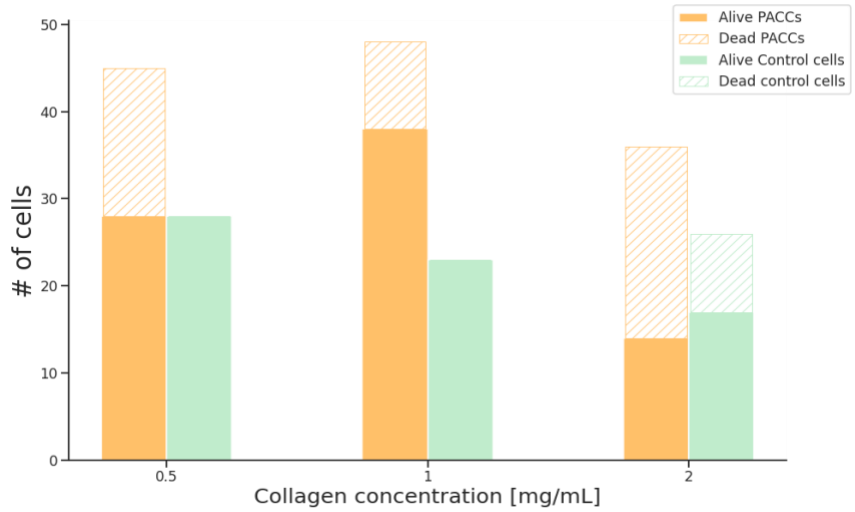

Figure 23: Quantification of number of living (solid color) and dead (shaded color) cells in various collagen concentrations. All PACCs data is shown in orange, control cells are in green. for 0.5 mg/mL n=2 exp, n=78 cells, for 1 mg/mL n=3 exp, n=71 cells and for 2 mg/mL n= 3 exp, n= 62.

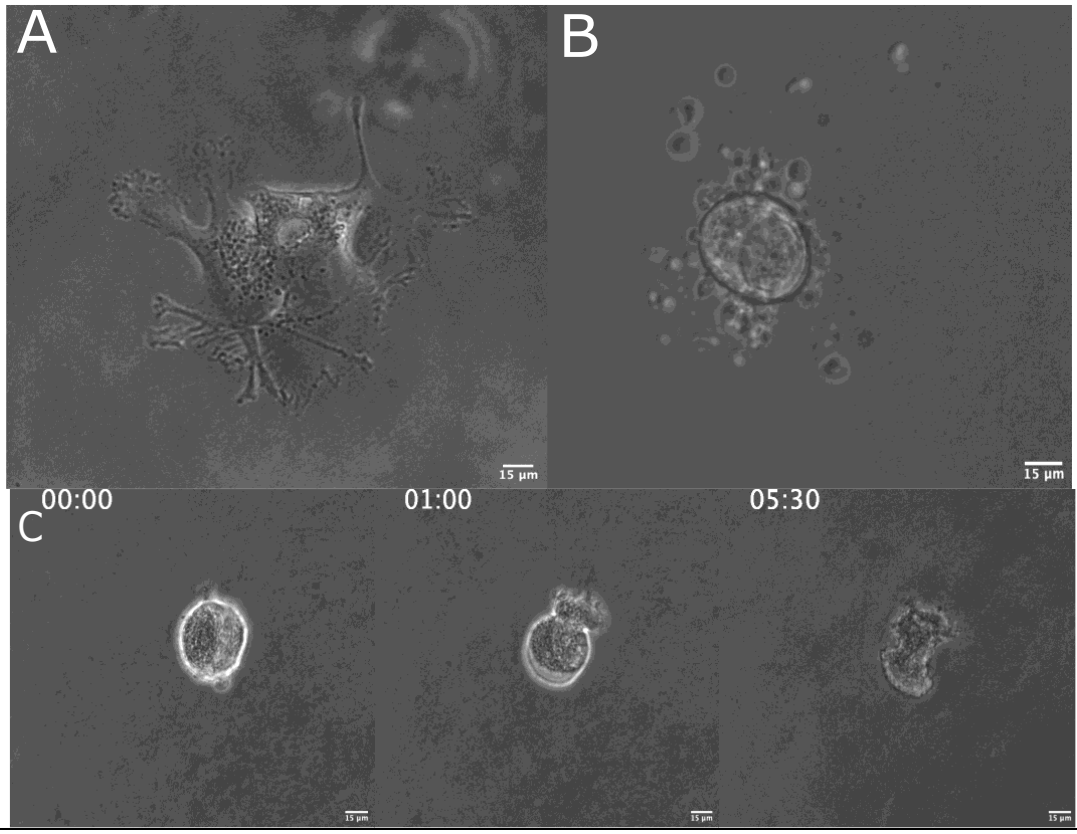

Figure 24: Examples of brightfield images from the time lapse microscope during the experiment. A) A brightfield image of a living cells with filopodia. B) A brightfield image of a dead cell. C) An example of how a control cell in 2 mg/mL can die during 18 hours the experiment. After 5 hours and 30 min the cell will dies, which the last image in figure C shows.

3.2 Quantification of cell division during encapsulation

To further verify the physiological relevance of each collagen condition, the percentage of cell dividing was quantified. Typically, cells divide when they reach M phase in the cell cycle. An example of how the control cells divide during the experiment can be seen in Figure 26D-F. However, PACCs do not divide at all at the selected stage of their development for imaging (Day 5). They are in paused cell cycle program and therefore are not quantifiable for this parameter. On the contrary, the control cells served as an indication that the 2 mg/mL collagen condition has the lowest percent of dividing cells at 29%, compared to 47.8% in 1 mg/mL and 43% in 0.5 mg/mL (Figure 25). The measurement of cell division is useful as a reference to the health of the cell line and the ability of the control cells to advance through the cell cycle. If nutrients can be distributed evenly in the collagen and cells can perceive a physiological environment, this could be an indication to not pause the cell cycle.

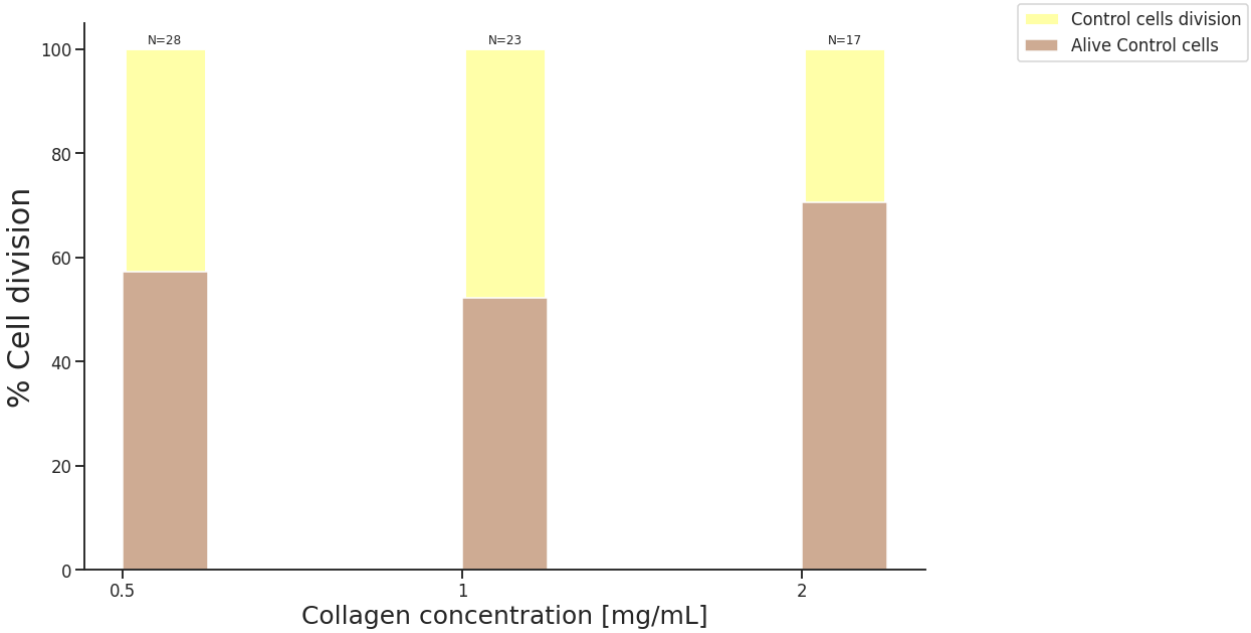

Figure 25: Quantification of dividing control cells (yellow) and non-dividing control cells (brown) in various collagen concentrations in %. The percentages for dividing cells in 0.5 mg/mL are 43%, for 1 mg/mL is 48% and for 2 mg/mL is 29%

3.3 Quantification of cell migration

3.3.1 Qualitative description of cells exhibition migration and migration-like behaviors

Cell migration is a challenging parameter to dissect quantitatively, as it is comprised of many parameters and definitions. To begin with, the definition of migration was separated in two categories: the presence of “movement” and “less movement”. The “movement” category is defined as cell shape change over time plus the presence of filopodia arms (Figure 26A-C). Here is an example of a collected time point with cells displaying behavior defined as “movement” in a video format. The “less movement” category is defined as lack of cell death overtime and minor cell shape changes (such as minor membrane protrusions and ruffling, which cannot be qualified as the criteria of “movement”). Here are examples of what “less movement” is defined as.

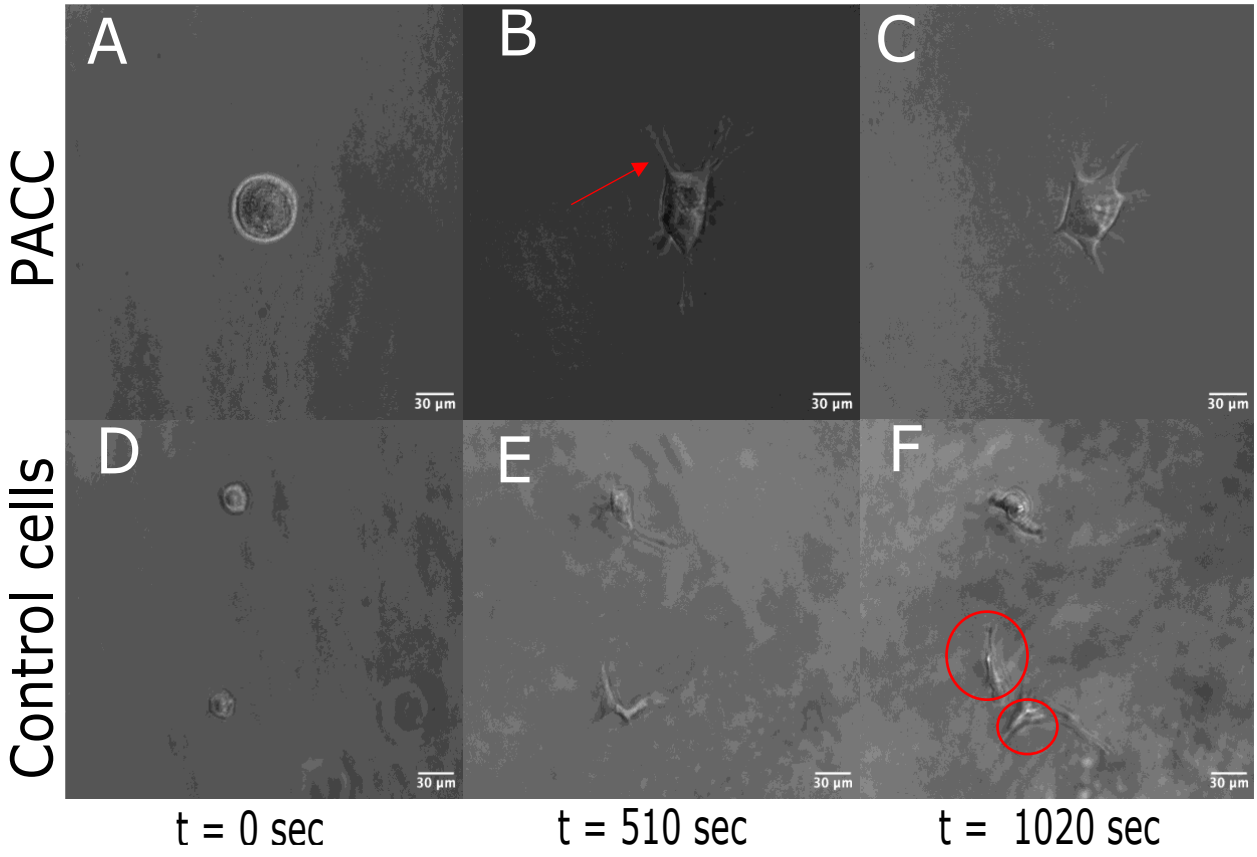

Figure 26: A timeline of the PACCs and control cells. A-C is for the PACCs in a 0.5 mg/mL collagen concentration. At t = 510 sec or 26B the PACCs begin to make long filopodia (arrow) D-F is for the control cells in 1 mg/mL. The circles demonstrate that the cells are dividing at the time t = 1020 sec or Figure 26F.

Figure 27 shows the percentage of how many cells display each of these behaviors. All control cells display the "movement" phenotype in 0.5 mg/mL, with progressively observing more of the "less movement" phenotype in 1 mg/mL. In 2 mg/mL the "less movement phenotype" becomes dominant. Similarly, this phenomenon is also observed for the PACCs. They demonstrate more movement in 0.5 mg/mL with 86% in comparison to 70% in 1 mg/mL, and in 2 mg/mL where they are 78% of the cells showing "movement" phenotype. Nonetheless, the PACCs' increase in percentage of cells that show "less movement" is still less drastic than the quantification for the control cells. The control cells switch from 100% "movement" in 0.5 mg/mL to nearly 100% "less movement" in 2 mg/mL. The results from the PACCs do not demonstrate such strong responsiveness to the environment. Even though I quantify an increase in the "less movement" cells, this increase is not significantly different to the one seen in the control cells.

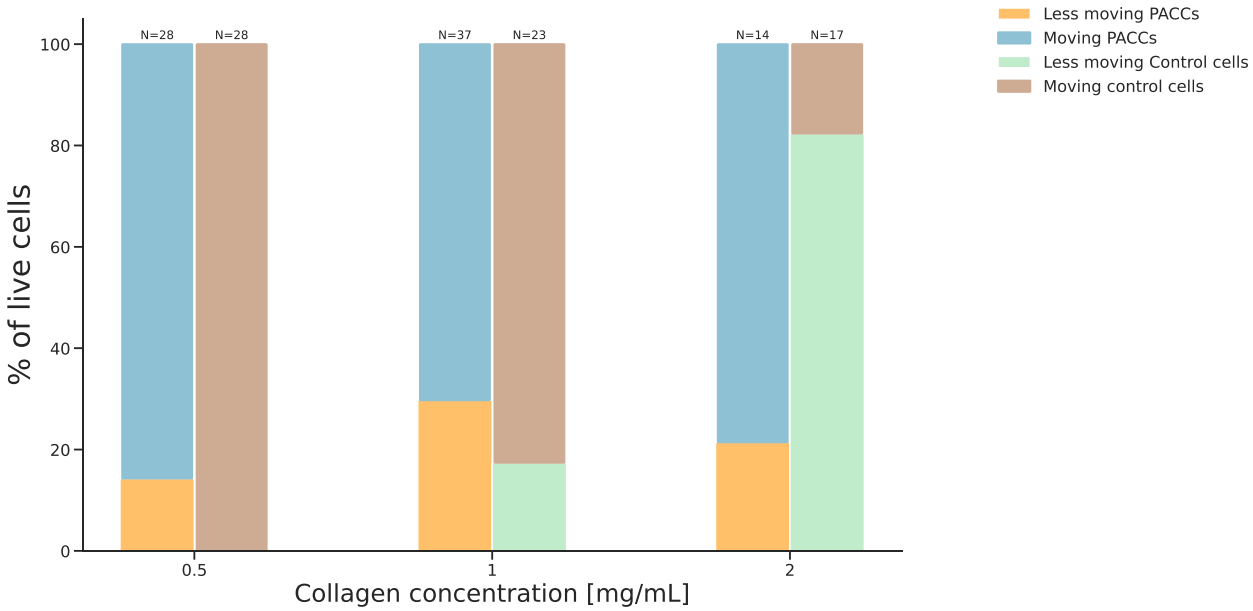

Figure 27: Quantification of cells that have “movement” or “less movement” for the control cells and the PACCs. PACCs in 0.5 mg/mL conditions have “less movement” (orange) with 14%, and 86% “movement” (blue). Control cells in 0.5 mg/mL have 100% “movement” (brown). In 1 mg/mL the PACCs have 30% “movement” and 70% “less movement”. The control in 1 mg/mL has 17% “less movement” and 83% “movement”. In 2 mg/mL the PACCs have 21% of “less movement “and 79% “movement”, and for the control it is 18% of “less movement” and 82% “movement”.

3.3.2 Quantitative analysis of cell migration

To investigate the cell’s capacity to explore its environment in greater detail that is not restricted to the two rather arbitrary categories defined above, a machine learning program was used for the aforementioned untreated PC3 cells and for the PACCs. The program analyzes individual images from a time-lapse movie. It converts them into a binary image by using Ilastik (The Interactive Learning and Segmentation Toolkit). This image is then used to perform tracking with the TrackMate plugin in Fiji. The conversion is needed for optimal cell segmentation. The TrackMate plugin then operates by finding the center of mass of each cell and tracking that position across the field of view until the final position is reached. Using this method, we can define the x and y coordinates of each cell within its recorded microscopy field of view. More details on the process can be found in Materials and Methods section. An example is shown in Figure 28, which illustrates the process.

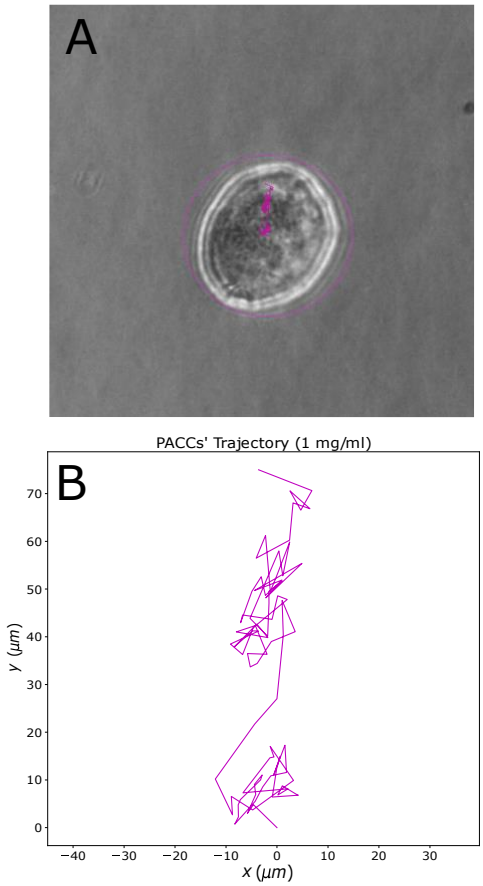

Figure 28: An example of the analysis process having the tracks and plotting the x and y coordinates. A) This is an example of a PACC's tracking from the plugin TrackMate in Fiji. Before the tracking was performed, the image was converted to a binary image (not seen here). B) A x and y coordinate system, where the dataset from the TrackMate is plotted. The tracking starts from the coordinate (0,0).

Figure 29 shows the detected cells' trajectories for each cell type (control and PACCs) in each collagen concentration. For the tracking all living cells were considered, so cells display both "movement" and "less movement" phenotypes. This was necessary as in some conditions if the "less movement" cells were to be excluded this would result in a non-analyzable dataset of 1-2 cell tracks. All trajectories are set to start at the same x/y position (0,0) on the plot. Using this type of cell track plotting, we can clearly visualize that the control cells have progressively shorter cell tracks with increasing collagen concentration. The cell trajectories in the 0.5 mg/mL condition cover a significantly larger area of the plot than in the 2 mg/mL condition, where the trajectories are collapsed in the center of the plot. This data confirms the previous qualitative description that the control cells demonstrate a high percentage of the "less movement" phenotype in 2 mg/mL collagen. The data also shows a trend between the change in collagen concentration and the change in motility phenotype, suggesting that higher collagen concentration could have a limiting effect on cell motility.

Similarly, the PACC's tracks also demonstrate a decrease in motility with increasing collagen concentration, with 0.5 mg/mL condition displaying the longest cell tracks moving furthest away from the center of the plot, compared to 1 and 2 mg/mL. However, here we can also clearly compare the behavior of the PACCs to the control cells, which show that overall, the PACCs move less than their control counterpart, covering shorter track distances. This result describes the difference in the PACCs versus control cells behavior much better compared to the qualitative analysis, which described which cells move "more" or "less". The result from the cell tracking analysis, however, shows that from the cells that did move, the PACCs still covered less distance compared to the control cells, which is a highly intriguing result. This result holds true in all three tested collagen conditions.

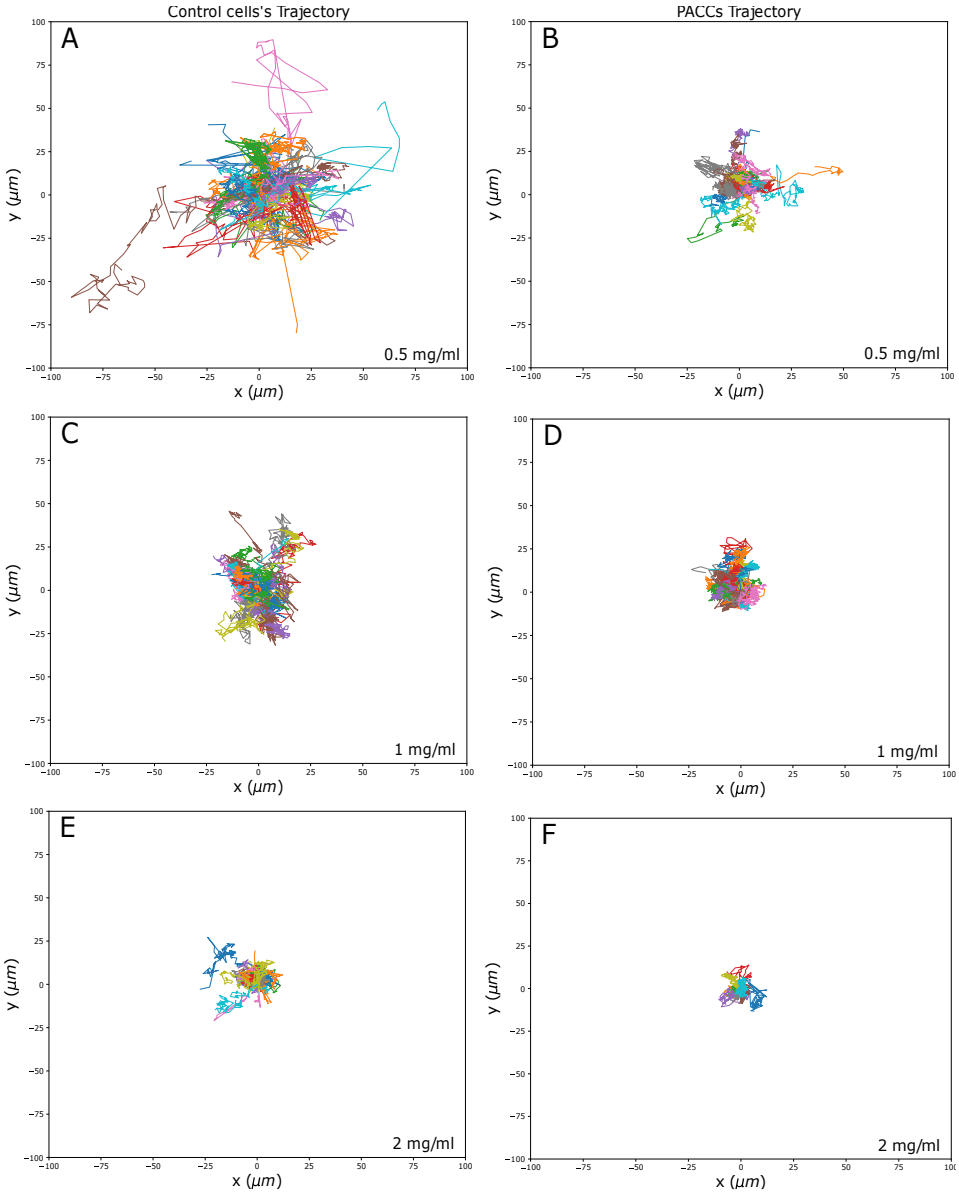

Figure 29: The cells' trajectory tracking for the PACCs and the control cells in all the different collagen concentrations. All tracks begin at (0,0) at t = 0 sec. A, C,E) is for the control cells and B,D,F) is for the PACCs.

Using these data, we formulate the hypothesis that the control PC3 cells move more than PACCs. **Employing an end-to-end (r_{ee}) distance plot we aim to test this hypothesis. At the same time, we will test quantitatively the qualitative observations from above figures of the results. Those are whether the PACCs' changes in movement over collagen concentrations are a plateau as reported from the qualitative analysis and whether the control cells show a strong linear trend with decreasing movement over increasing collagen concentration.**

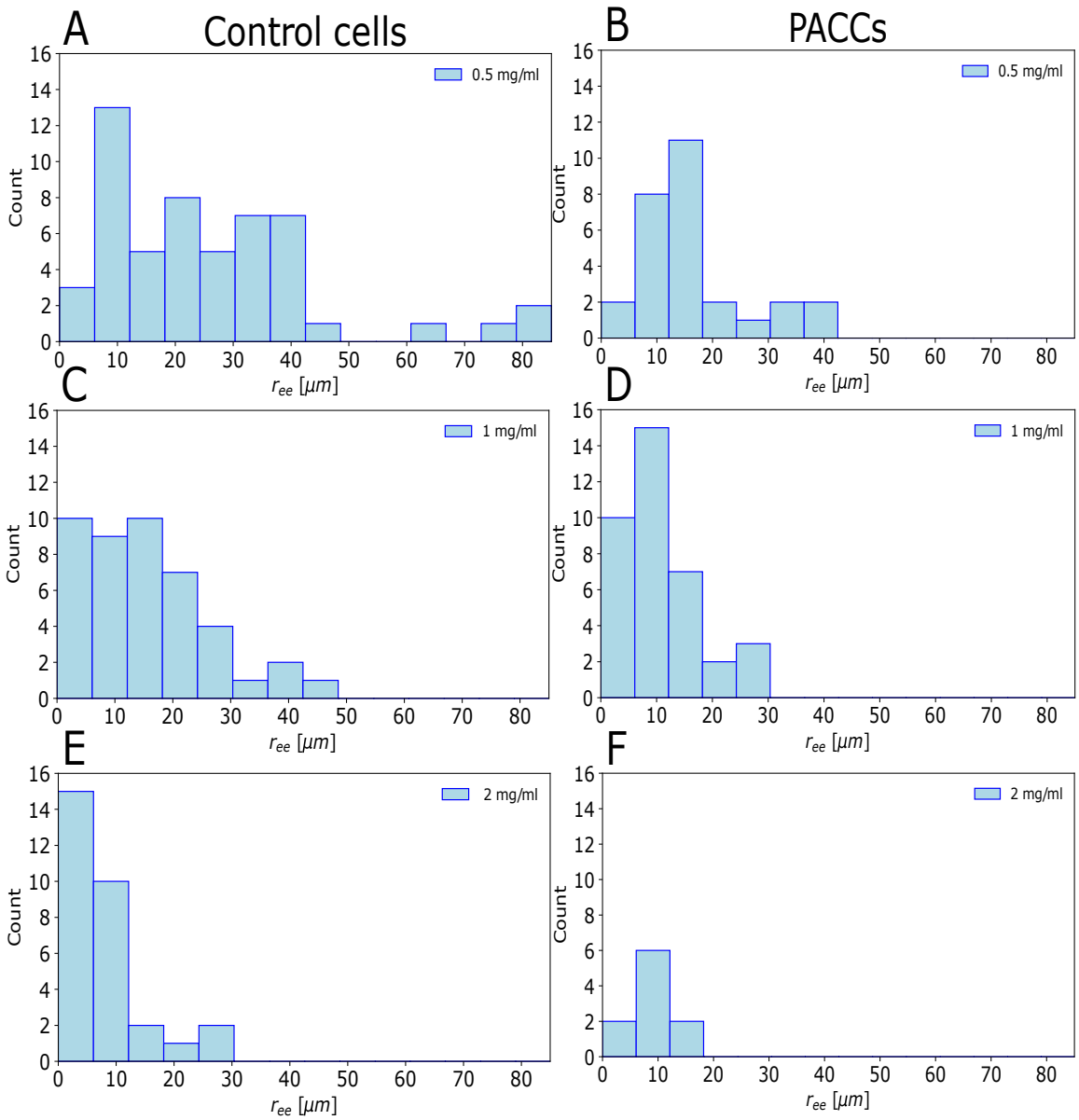

Figure 30: The end-to-end distribution of the number of tracks (count) versus the track length in microns (r_{ee}). This is made for the control cells (A,C,E) and for the PACCs (B,D,F). The first row is for the 0.5 mg/mL collagen concentration, the second row 1 mg/mL and the last is for the 2 mg/mL.

To either reject or confirm our hypothesis, firstly the r_{ee} distance for each track was determined, which is the distance from the first position to the end position of the track. Figure 30 shows the distribution of the number of tracks (count) that display a certain track length (r_{ee}) as defined in eq. 5. This analysis reveals that with increasing collagen concentration, the distribution of r_{ee} distances for the control cells strongly shifts towards shorter distances of up to 30 µm, while the 0.5 mg/mL condition has cell tracks distribution of up to 80 µm. When comparing control cells to PACCs, we find an interesting result that the number of short track distances of up to 10-15 µm is comparable, while the number of mid-range tracks of 20 to 40 µm strongly decreases for the PACCs. Even though long-range tracks above 40 µm are also rare for the control cells (only counted one or maximum two tracks per distance length), they are completely non-existent for the PACCs in any of the collagen conditions.

The standard deviation for each r_{ee} distance was calculated and plotted in Figure 31, where all the trajectories for the control cells and PACCs were summed up to find the mean value of the r_{ee} distance per collagen condition. On this plot we can clearly see that the mean r_{ee} distances for the control cells are steadily declining with increase of collagen concentration, while the PACCs track distances decline between 0.5 and 1 mg/mL and then plateau between 1 and 2 mg/mL. Figure 31 also shows the standard deviations for each r_{ee} track distance mean value. For both cell types, the standard deviation decreases with increasing collagen concentration. The standard deviation is a quantification of the biological variation within a system. High standard deviation is an indication of high variability in the tested system. In this case, the highest standard deviation is seen for the 0.5 mg/mL collagen condition, where the cells demonstrate the widest distribution of r_{ee} distances of their tracks.

This result is consistent with the observation that more cells exhibit motility at this condition and therefore a wider plethora of behaviors has been recorded. Conversely, at high collagen concentrations, there was limited movement, fewer moving cells and from the cells that did move, they covered shorter distances and therefore the distribution of their biological behaviors is more limited.

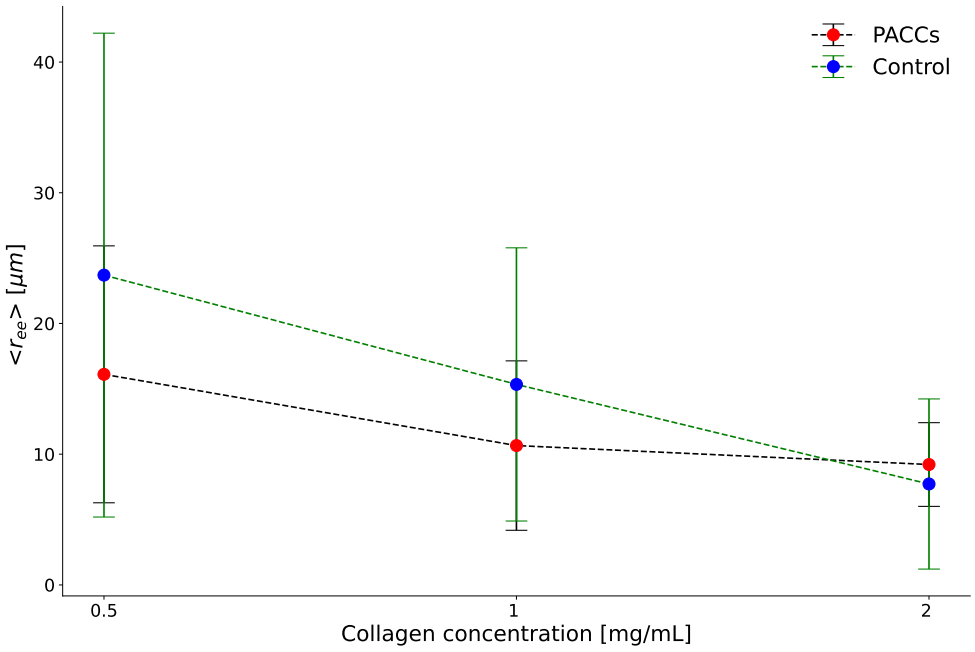

Figure 31: All the trajectories for the control cells and PACCs summed to find the mean value of the r_{ee} distance per collagen condition. The error bars represent the standard deviation.

The plot of the mean values of the r_{ee} track distances in Figure 31 show that the biggest numerical difference is between PACCs and control cells in 0.5 mg/mL condition (16.11 μm and 25.7 μm, respectively). In order to understand whether this difference is meaningful, the statistical significance was estimated. To select the appropriate statistical significance test, the distribution of the data has to be considered for normality (normal distribution or not). For instance, a normal data distribution would justify the use of a test, such as the student t-test, but a non-normal distribution would require the use of a non-parametric test. The test for checking the normal distribution of the data showed that the control cells have a p – value = 0.00018, which is below the 5 %, and therefore the dataset is not normally distributed. The PACCs had p-value of = p = 0.042, which also indicates that they are not normally distributed. These results justified the use of a non-parametric test for two populations that similarly to each other have a non-normal distribution. The Mann-Whitney is a U test for comparing independent data samples. Comparing the data for the control cells and PACCs in 0.5 mg/mL condition using the U-test resulted in a p-value of 0.024, which indicates that we can reject the null-hypothesis that they are equal to each other. Therefore, the control cells do move significantly more than the PACCs in the 0.5 mg/mL collagen concentration condition.

The r_{ee} distances were also used to estimate the ensemble-average mean squared displacement (MSD). Firstly, the data was fitted with $K_\alpha * \tau^\alpha$ (eq.4), where α represents the anomalous coefficient. In order to allow for most precise fitting, the following data alignments were performed.

1.Throughout the duration of the time-lapse cells begin their movement at different time points. Therefore, all tracks were shifted and aligned to start at time point t=0 sec.

2. At the same time, cells move for a different length of time as indicated by the presence of increasing noise along the blue line in Figure 32 – i.e. some cell track durations are 30mins, while others are 300 min.

Therefore, a cut-off was made after the first 10 time points (100 min) to allow same-conditions comparison of the fitting analysis for each concentration. To clarify, as the time interval between each time point is 10 min, the cut-off at 10 time points is equal to 100min or 1.6 hours.

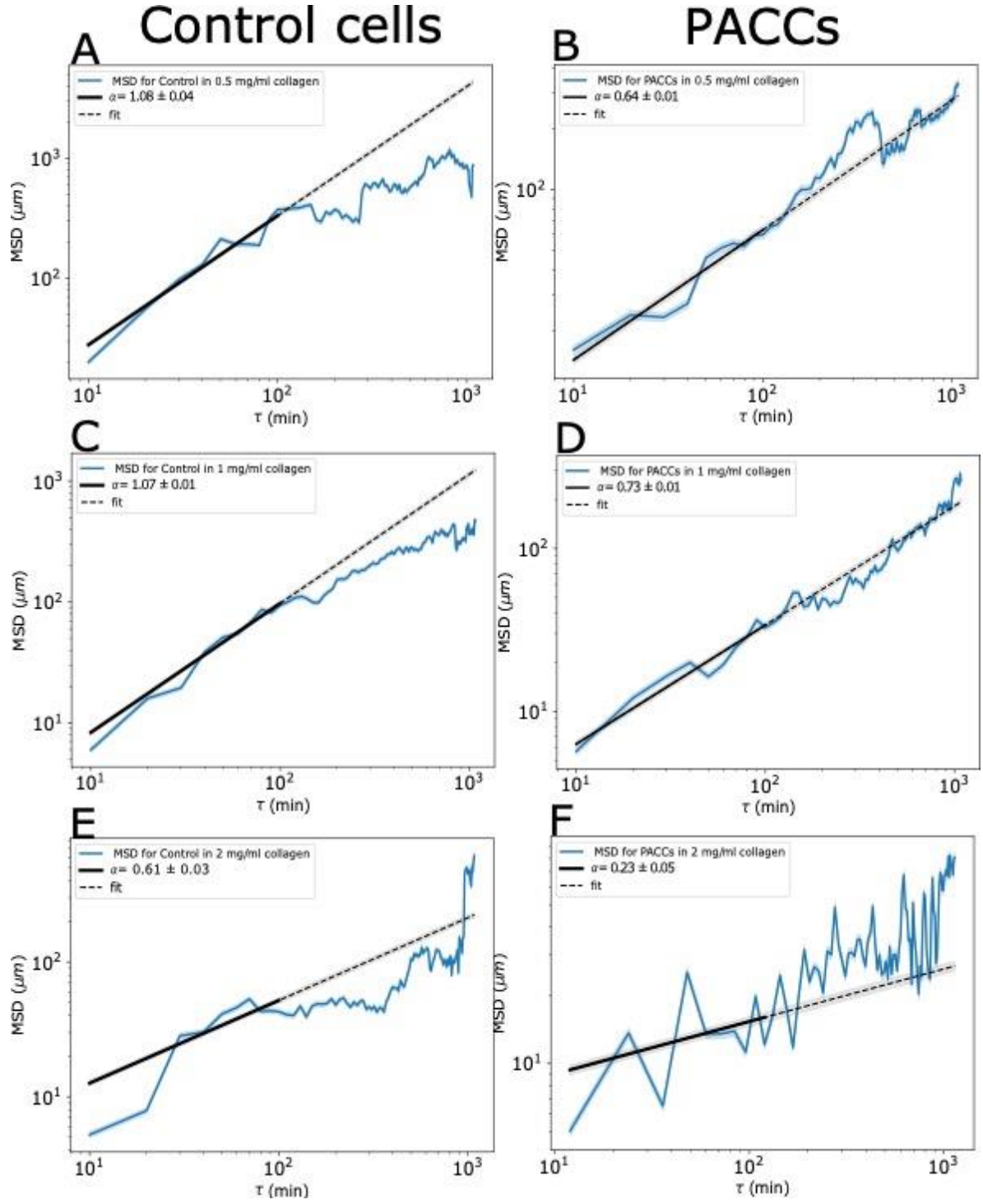

Figure 32: EA MSDs for the three collagen concentrations for the PACCs (B, D, F) and control cells (A, C, E). The six EA MSDs were fitted into a linear equation to obtain the values of the anomalous α exponents. The dashed line represents the fitting, and the marked black line is the data, which were fitted to the linear equation.

The 100 min cut-off includes 9% of all the existing tracking data that is used to fit it to the MSD. Even though this is a small amount of data, the cut-off was necessary because of the increase in noise over time could result in the wrong detection of anomalous types of diffusion due to the

noise artefact. Here, it was important to make sure that we investigate the results from only correctly fitted MSD.

Next, after fitting the data, we can examine the relationship between the MSD and time and see whether it is a linear or non-linear relationship (Figure 32). A linear relationship indicates a normal diffusion (Brownian motion) and a non-linear relationship describes the so called anomalous type of diffusion that can be either subdiffusion or superdiffusion. Using the fitted lines on our MSD data, we can extract the values for α, which describe the type of diffusion.

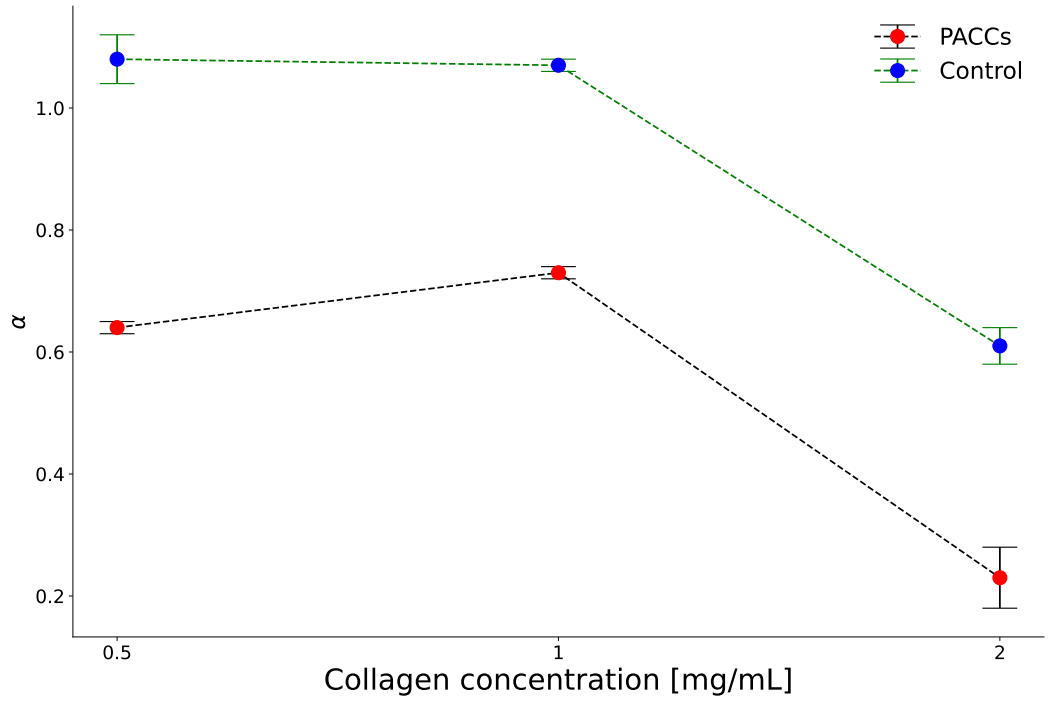

Figure 33: The relationship between the anomalous α coefficient and the three collagen concentrations. The number of α can be seen in Table 2. The error bars represent the standard deviation.

Table 2 for the anomalous diffusion coefficient from the MSD for the r_{ee} distance. Variation is found by with a 5 % confidence interval.

Concentration	Control cells	PACCs
0.5 mg/ml	1.08 +/- 0.04	0.64 +/- 0.01
1 mg/ml	1.07 +/- 0.01	0.73 +/- 0.01
2 mg/ml	0.61 +/- 0.03	0.23+/- 0.06

The control cells in 0.5 mg/mL and 1 mg/mL have a diffusion constant of 1.08 +/- 0.04 and 1.07 +/- 0.01 which corresponds to a normal diffusion or a Brownian-like motion. The control cells in 2 mg/mL are categorized instead as subdiffusive as they have an anomalous diffusion coefficient at 0.61 +/- 0.03. Interestingly, the PACCs show subdiffusion coefficients for all tested collagen conditions. Still, similarly to the control cells, the 2 mg/mL condition produced by far the lowest α value of 0.23 +/- 0.06. (Figure 33, Table 2) These results are highly interesting as further explored in the Discussion section, because if we apply the definition of subdiffusion to this context, it would entail that the cells are not moving due to random trapping in their environment. This indicates that the environment of 0.5 mg/mL and 1 mg/mL was non-trapping for the control cells, but it was trapping for the significantly larger PACCs.

3 Discussion

Contrary to the suggested hypothesis, the results of the study demonstrate that PACCs exhibit no significant motility in 3D environments. The hypothesis that PACCs exhibit more movement in a 3D environment or even a special kind of migration in 3D was based on PACCs' mesenchymal migration on 2D surfaces. This was also coupled with the suggestion that a 3D gel encapsulation would present an environment closer to the one cancer cells experience *in vivo* as it delivers physical constraints signaling the cell that it is in a tissue-like environment.

Nonetheless, the results presented here from the higher number of cell death for PACCs in collagen. If we compare this to the control cells to the clear quantification of shorter tracking paths and subdiffusion diffusion coefficient values clearly speaks to the impaired motility of the PACCs in this 3D environment. In order to understand the root of this discrepancy, we have to consider a number of highly important effects of the generated environment the cells are in.

Firstly, we have to consider the choice of gel material – collagen – and whether this choice offers an optimal environment for the study. Collagen type 1 was selected for the following reasons. Firstly, it is a standard material to produce 3D gels for cell encapsulation [50,51,52]. Secondly, a study comparing collagen and Matrigel gels in 2D and 3D suggests that collagen is a better substrate when studying invasive cancer cell types [53]. This is due to the fact that cells need to interact with collagen to overcome basement membranes and stromal matrices *in vivo* in order to metastasize [53]. The study revealed that Matrigel cannot form representative barriers similar to the ones *in vivo* as well as collagen and was suggested as the superior substrate when

studying invasive cancer behaviors. Finally, the specifically used collagen 1 brand and concentration for this study, was already tested for the encapsulation of aggressive cancer cell types that also have capacity to form PACCs in a study of the effect of the 3D gel on the cell motility [49].

Nevertheless, seeing the extreme effect of the collagen on the PACCs, it would be highly beneficial to test either a different brand and polymerizing agents for the collagen or another commonly used material, such as Matrigel. Slight technical differences can produce strong changes in biological behaviors; therefore, we first need to consider in depth the type, brand, and concentration of collagen used. Even though collagens should be similar, each brand collects and distributes it using slightly different reagents. This determines that different collagen brands need to be prepped for polymerization using a different mixture of neutralizing agents. This means that different collagen preparations will result in different polymerizations and therefore different collagen gel stiffnesses. For example, the collagen used in this study FirstLink rat-tail collagen 1, was used in five studies in concentrations of 2 mg/mL, neutralized NaOH was considered to be physiological for the studied variety of five different cell types [44,45,46,47,56]. The stiffness of this gel preparation, however, was never measured using optical tweezer methodologies, as was done for other collagen preparations. In the paper by Wullkopf et al., 2018 [48], the Corning brand collagen was used (personal communication with the author) and was neutralized using a mixture of HEPES, $NaHCO_3$ and MEM medium to produce a 1 mg/mL collagen concentration. This specific preparation was tested using optical tweezers to quantify a Young's modulus of $Y = 377 \pm 68$ Pa. This value corresponds well to values of healthy soft tissues such as the lung or mammary glands [54]. Nonetheless, we cannot assume that the 1mg collagen preparation in this study will have the exact same Young's modulus due to the differences in collagen gel preparation. For all these reasons, it would be important to either test the same used concentrations using the other collagen concentration as was tested in the literature or to perform a measurement of the Young's modulus for the collagen preparations used in this study.

Even though the Young's modulus of the 3D gels used here were not individually quantified, we used measures of the cell behavior to ensure that the environments were non-hostile for cell survival, growth, and motility. This was done by using the control cells PC3 encapsulation as a positive control. PC3s are a well-studied motile and aggressive type of prostate cancer. In 0.5 mg/mL and 1 mg/mL conditions, these cells showed none of minimal cell death and a high percentage of cell division, which indicates that the cells were not stressed in these collagen concentrations and could go through their cell cycle. In addition, PC3s had significantly longer

track lengths and displayed at the minimum a Brownian-like motion. This suggests that the collagen preparations were not by themselves limiting to cell survival and movement. Nonetheless, the PACCs underwent cell death more often than the control cells and moved significantly less and at lower distances at 0.5 mg/mL and 1 mg/mL.

This behavior could be due to different parameters: larger cells' inability to transverse within gel environment with a certain stiffness and porosity, PACCs biological response to presence of collagen (receptor-based detection of collagen causing morphology change and a block of motility pathways), and effects of the collagen on the PACCs among others.

Let us consider the effects of the gel concentration on the cell movement. Using the plot of the mean-square displacement, the anomalous diffusion coefficient, α, was estimated for the movement of each cell type (control and PACCs) for each collagen condition. For cells and/or biological entities that exhibit motile behaviors due to active processes utilizing energy, the expectation would be for an estimation of $\alpha > 1$, or a superdiffusive type of behavior [36,37]. None of the measured cells showed a superdiffusive behavior, however. The control PC3 cells demonstrated clear motility patterns in 3D visible by eye in 0.5 mg/mL and 1 mg/mL conditions as recorded in the qualitative analysis with 100% and 82% of the cells having the "movement" phenotype respectively. While the PC3 cells in these two collagen concentrations also had the longest r_{ee} distance of track lengths (Figure 30), the cells had a normal diffusion ($\alpha = 1$) that could be equated to a random-walk Brownian-like motion. However, diffusion is dependent not only on the forces exerted by the living system, but also on the forces exerted by the physical environment on the cell itself. In this regard, if we compare the 0.5 mg/mL and the 2 mg/mL condition, the 2 mg/mL collagen could provide a stiffer, denser environment, or an environment with lesser porosity that could prevent the cells from moving as freely. Even though we have not quantified any of the physical parameters of each gel preparation, the fact that the control cells in 2 mg/mL show a subdiffusive behavior compared to the cells in 0.5 mg/mL and 1 mg/mL is an indication of an increasingly restrictive gel environment that progressively limits motility. The definition of subdiffusion is that the molecules (or cells in this case) display a diffusion below Brownian-motion due to random entrapment by the environment [55], which indicates a clear relationship between the motile entity and its environment. Importantly, all measured cell behaviors – death, division, and motility – scaled with the change in collagen concentration in a manner suggesting that the increasing collagen provides a more restrictive environment causing higher cell death, decrease in cell division, and motile behaviors. In this train of thought, since the control PC3 cells which do display motility, but only a normal diffusion $\alpha = 1$, the cells might

need an even “softer” collagen environment in order to show migration that corresponds to superdiffusive values of α >1 as is the expectation for energy-dependent processes. This suggests that the testing collagen environments below 0.5 mg/mL could be an intriguing continuation in future research. In it important to note that there are more direct methods for the quantification of diffusion coefficients, such as FRAP (fluorescence recovery after photobleaching) where a cell is fluorescently tagged, subjected to photobleaching via laser and the recovery of signal is recorded over time [57]. This method can be used as a complement experiment to validate the diffusion coefficients quantified here.

Nonetheless, using the data produced in this work, intriguingly, the PACCs’ cells MSD diffusion coefficient quantification indicates that the PACCs experience environment entrapment as indicated by α <1 in all collagen conditions (subdiffusive behavior). What are the reasons for this highly motile in 2D cell type to experience a sharp phenotypic change?

The quantification of cell death events for the PACCs indicate that all presented collagen conditions from 0.5 mg/mL to 2 mg/mL are more detrimental for the PACCs in comparison to the control cells, as they experience more cell death events (Figure 23). The PACCs themselves are cells under stress, with paused cell cycle and abnormal genetic content, however, these parameters were considered to be in some way related to the emergence of the cell’s resistance. In this study, it appears that the PACC is more “sensitive” to the 3D environment compared to the more “robust” control cells. PACCs experience more cell death (Figure 23) and more limited movements with fewer cells qualifying for the qualitative group of “movement” (Figure 27) and with track-lengths end to end distances clearly indicating a very limited short track length (Figure 30). When visually observing these cells, the majority of them are only able to explore the environment through the formation of filopodia, but very few cells physically move across the field of view.

Some hypotheses could suggest that: 1. The larger PACCs are unable to transverse the collagen matrix due to its stiffness and porosity, which limit the cell’s capacity to physically move through the gel; 2. Inhibition of motility through change of PACC morphology in a 3D collagen environment; 3. Inhibition of motility due to the presence of collagen itself.

If the cells are unable to move simply due to a physical restriction, this can refer to the ability of cells to detect the softness of their physical environment as in article by Lomakin et al, 2020 [58]. Using the larger or smaller extent of deformation of the cell nucleus membrane as a result of a

stiffer or softer environment, respectively, a cell is able to detect its 3D surroundings [58]. For instance, if we take the example of our PC3 control cells, which are smaller than the PACCs and with a small nucleus a change from 0.5 mg/mL to 2 mg/mL of collagen can present a significant shift in the detection of the stiffness and as a result the cells display a wider range of behaviors (strong shift away from “movement” phenotype, sharp increase in cell death in 2 mg/mL collagen, etc.). However, due to the incredibly large cell sizes for PACCs, and their large individual nuclei or potentially multi nuclei, it is conceivable to consider that the stiffness of the collagen in the tested concentrations could not exert sufficient force for the cell to detect any meaningful deformation and respond accordingly. Potentially, the test range of collagen was too narrow and the PACCs require a wider difference in order to detect a threshold in the change of the environment. If the stiffness of the high collagen is therefore insufficient to cause deformation, a higher than 2 mg/mL collagen concentration should be tested. However, it is important to note that already in 2 mg/mL collagen, the PACCs are experiencing significant cell death, suggesting it to be an unfavorable environment. On the other hand, if the cells are confined in a sufficiently stiff environment in the current tested conditions to detect deformation but are unable to move through the collagen gel matrix due to their large size being limited by the polymer matrix, it will be valuable to test lower than 0.5 mg/mL collagen concentrations. Ultimately, in order to answer the question how would a PACCs respond *in vivo*, one must test the Young’s modulus of the currently “best” condition 0.5 mg/mL collagen (lowest levels of cell death, and highest levels of movement) and compare the stiffness of that gel to a tissue environment. Based on that quantification a meaningful analysis of the current data can be done along with a suggestion for the improvement of the 3D gel.

At the same time, we must consider the presence of molecular pathways that can respond to the new challenge of interacting with a 3D collagen gel. Firstly, the collagen itself could be a restrictive substrate to the cells. Therefore, experiments in our collaborating lab in Lund are undergoing in which the PACCs are presented with a 2D collagen surface. The PACCs are known to be motile in 2D, so will they be motile in a 2D collagen plate? Does the issue of lack of motility arise at the level of the 3D encapsulation or much simpler at the interaction with collagen? Another possibility is that the PACCs present receptors that can detect the presence of collagen and trigger molecular pathways to block motility when encountering this specific substrate.

These hypotheses are highly relevant to answer the question of whether PACCs in this part of their development (Day 5), actually can and would exhibit motility *in vivo* in the organism as they do in 2D laboratory conditions. As discussed above, collagen was selected also due to the fact

that it generates *in vitro* a much more natural barrier as the ones observed *in vivo* at basement membranes crossed during cancer cell metastasis. If PACCs have pathways blocking their motility when collagen is encountered this could be telling of their life cycle in the organism. For example, a Day 5 PACC is large, resistant to treatment, and growing in genetic material. Its size could simply not be able to be sustained in motion by its cytoskeleton. Eventually, from Day 12 onwards, this PACC will produce numerous resistant daughter cells, much smaller in size and also as observed in 2D – motile. I would like to suggest a counter-hypothesis to the one presented in the introduction, now based on the current results that the large Day5 PACCs do not need to exhibit movement at that stage in a 3D environment. They can extend filopodia to "scan" their environment, but the energy needed to drive a cell of this tremendous size through a dense tissue while it continues to grow count be detrimental to the successful dissemination of the cancer. Instead, this large "mother" PACC could potentially remain immobile and resistant to the treatment until it exits quiescence and enters the phase of production of "daughter" cells, which are smaller and could more easily transverse the primary tumor environment. It would be incredibly interesting to perform the same gel entrapment experiments with the PACCs daughter cells produced after day 12 of treatment to test whether the same collagen environment affect those cells similarly as the large PACCs.

4 Future Outlook

Below I present some meaningful ways in which the current research can be expanded on:

1. Studying the velocity and dynamics of the PACCs. Using the suggestions from the Discussion section on clarifying the influence of the collagen itself and selecting the optimal gel concentration to test for motility, the next step would be to better define the velocity and the dynamics of the PACCs. The velocity quantification could be done by using the MSD, which contains a velocity autocorrelation function (VACF) information. In the current study, no meaningful translocation of individual PACCs for a sufficient number of cells was available to conduct this quantification, however, finetuning the environment could provide a great opportunity for similar quantifications, considering that the PACCs exhibit a motility in 3D. Being able to record cells exhibiting clear motility will also provide an opportunity to dissect the question of the type of exhibited PACC dynamics in 3D and whether they prefer amoeboid or mesenchymal types of migration. In 2D the migration is mesenchymal, and so far, the observations in 3D have been that the PACCs form long filopodia to explore their immediate

surroundings. This could indicate that mesenchymal migration pathways are present and utilized in 3D environments as well. Nonetheless, the suggested experiments as in Discussion section of further reducing or increasing the collagen concentration will provide a different environment stiffness for the cells. Decreasing the collagen concentration sufficiently could even result in reduction of the surface contacts with the cell and ultimately result in a shift from mesenchymal to amoeboid types of migration.

2. In order to properly assess the types of exhibited migration and to better visualize the cell in motion, an ideal experimental continuation is the fluorescent tagging of cytoskeletal and membrane components of the PACCs via transfection and their observation via fluorescence or laser microscopy. For instance, in order to differentiate between mesenchymal and amoeboid migration types, tagging actin filaments would be beneficial to visualize whether filopodia extensions are formed or rather for amoeboid migration actin is organized only internally (acto-myosin cortex and internal actin filaments). Ultimately, different cell motility behaviors are determined by the spatio-temporal interplay between three factors that serve as the molecular basis for different cell motility: adhesion, the actomyosin cortex, and actin polymerization [4]. Therefore, an analysis of the dynamics of these cell features using fluorescence tagging and microscopy over time, so the contribution of each factor can be assessed is an exciting future avenue for the enrichment of this project. Cell tagging could have already been used in the current study to quantify the observed filopodia lengths for the control PC3 cells and their PACCs. An interesting quantification here would be to estimate the ratio of filopodia length to cell size. For example, do the control cells which are able to move across the field, do they develop longer filopodia comparative to their cell size, which provide sufficient force to translocate the cell from point A to point B? Are the PACCs unable to form sufficiently long filopodia in order to move them and would they need longer filopodia when moving a larger cell size? A fluorescence imaging and analysis is preferred to the brightfield (BF) imaging performed here, since from brightfield images neither used plugin TrackMate nor Ilastik could segment the filopodia due to their lack of precision in segmentation and the easier loss of filopodia in BF 3D.

3. Investigation of chemotaxis for PACCs. So far, the research presented here has been focused solely on the physical environment and constraints presented to the PACCs in their shift from 2D to a 3D environment. This line of experimentation until now has disregarded the fact that the cells are embedded in a complex tumor environment, surrounded by neighboring cancer and healthy cells, ECM, blood vessels, etc. The PACCs therefore, do not exist in

isolation and receive multiple chemical and molecular stimuli from the neighboring cells. In the case that no specifically “optimal” collagen gel concentration is found on its own to trigger PACCs motility, we should consider the possibility that molecular stimuli could be needed for motility, in which case PACCs would display chemotaxis motility behavior. If the environment on its own is insufficient, then how would the PACCs behave if they were introduced in a gel encapsulation together with sister cells, even higher concentration of PACCs, PACCs in later stages, known as daughter PACCs, or in the presence of healthy tissue cells? These are incredibly exciting pairings of cell types for the dissection of the contribution of each of these cell types to the tumor microenvironment.

4. The entire study uses only the prostate cancer cell line PC3. As mentioned in the introduction, however, PACCs can be generated from a variety of cancer with great success. As a long-term perspective, it would be very interesting to compare the dynamic behaviors of PACCs derived from different cancer cell lines in order to understand if the PACCs retain any of the behaviors and signatures of the original cell line, or rather they have “evolved” into an entirely new cell type, where PACCs are more similar in behavior, cell and molecular biology to each other rather than to the original cancer cells. It would also provide a great opportunity to test PACCs derived from different cancer cell lines in different gel environments – i.e. collagen versus Matrigel – and infuse those gels with molecular signatures particular to the original tissue environment of each cancer cell.

5 Conclusion

The project in this Master thesis addresses a novel and exciting cancer cell type that can be the precursor cell for cancer metastases: the poly-aneuploid cancer cell (PACC). This chemotherapy and treatment resistant cell type was discovered to display motility on 2D surfaces soon after its generation, however, the experiments conducted here suggest that the cell present a different behavior in 3D. Switching from actively motile to only exploratory behavior using filopodia, the extremely large PACC cell seems unable to freely transverse the presented collagen gel environment in which the cell is encapsulated. The objective was to test the hypothesis whether when presenting those cells with an environment more closely resembling a tissue environment this will stimulate further their migration and/or force them to exhibit different types of migration. The results, however, suggest a reconsideration of the original hypothesis. I propose a new direction for future work on the topic and that is to explore whether the extremely large resistant PACCs from Day 5 of treatment are able to exhibit any movement in 3D, or that would be too costly process due to their tremendous size, and therefore, motility for PACCs is reserved to the offspring: the PACC daughter cells. Testing this new hypothesis will provide a wide variety of experimentation where the entire life cycle of the PACCs can be tested for emergence of motility in 3D. This will be highly beneficial research for the broad field of cancer biology, where the PACCs cell type has been overlooked for the past 100 years due to its rarity and unique morphology. The discovery of this cancer cell type, and its analysis using advanced quantitative imaging approaches as 3D encapsulations and live-imaging will allow the fast and meaningful dissection of the unique molecular pathways of the PACCs with one end goal – to prevent them from moving and propagating secondary tumors and metastases.

6 Bibliography

1. Bendell, A. C., Anderson, N., Blumenthal, D., Williamson, E. K., Chen, C. S., Burkhardt, J. K., & Hammer, D. A. (2018). Motile Dendritic Cells Sense and Respond to Substrate Geometry. *Annals of Biomedical Engineering*, *46*(9), 1348–1361. https://doi.org/10.1007/s10439-018-2041-7
2. Piipponen, Minna et al. “The Immune Functions of Keratinocytes in Skin Wound Healing.” *International journal of molecular sciences* vol. 21,22 8790. 20 Nov. 2020, doi:10.3390/ijms21228790
3. Miao, Y., Bhattacharya, S., Edwards, M., Cai, H., Inoue, T., Iglesias, P. A., & Devreotes, P. N. (2017). Altering the threshold of an excitable signal transduction network
4. Paterson, N., & Lämmermann, T. (2022). Macrophage network dynamics depend on haptokinesis for optimal local surveillance. *ELife*, *11*, e75354. https://doi.org/10.7554/eLife.75354
5. Paul, C. D., Mistriotis, P., & Konstantopoulos, K. (2017). Cancer cell motility: Lessons from migration in confined spaces. *Nature Reviews Cancer*, *17*(2), 131–140. https://doi.org/10.1038/nrc.2016.123
6. Patel, A. (2020). Benign vs Malignant Tumors. *JAMA Oncology*, *6*(9), 1488. https://doi.org/10.1001/jamaoncol.2020.2592
7. Martin, T. A., Ye, L., Sanders, A. J., Lane, J., & Jiang, W. G. (2013). Cancer Invasion and Metastasis: Molecular and Cellular Perspective. In *Madame Curie Bioscience Database [Internet]*. Landes Bioscience. https://www.ncbi.nlm.nih.gov/books/NBK164700/
8. Hanahan, D., & Weinberg, R. A. (2000). The Hallmarks of Cancer. *Cell*, *100*(1), 57–70. https://doi.org/10.1016/S0092-8674(00)81683-9
9. Hapach, L. A., Mosier, J. A., Wang, W., & Reinhart-King, C. A. (2019). Engineered models to parse apart the metastatic cascade. *Npj Precision Oncology*, *3*(1), 20. https://doi.org/10.1038/s41698-019-0092-3
10. Shieh, A. C. (2011). Biomechanical Forces Shape the Tumor Microenvironment. *Annals of Biomedical Engineering*, *39*(5), 1379–1389. https://doi.org/10.1007/s10439-011-0252-2
11. DeVita, V. T., & Chu, E. (2008). A History of Cancer Chemotherapy. *Cancer Research*, *68*(21), 8643–8653. https://doi.org/10.1158/0008-5472.CAN-07-6611
12. Pienta, K. J., Hammarlund, E. U., Brown, J. S., Amend, S. R., & Axelrod, R. M. (2021). Cancer recurrence and lethality are enabled by enhanced survival and reversible cell cycle arrest of polyaneuploid cells. *Proceedings of the National Academy of Sciences*, *118*(7), e2020838118. https://doi.org/10.1073/pnas.2020838118
13. Dasari, S., & Tchounwou, P. B. (2014). Cisplatin in cancer therapy: Molecular mechanisms of action. *European Journal of Pharmacology*, *740*, 364–378. https://doi.org/10.1016/j.ejphar.2014.07.025
14. Guo, Q., Lan, F., Yan, X., Xiao, Z., Wu, Y., & Zhang, Q. (2018). Hypoxia exposure induced cisplatin resistance partially via activating p53 and hypoxia inducible

factor-1α in non-small cell lung cancer A549 cells. *Oncology Letters*, *16*(1), 801–808. https://doi.org/10.3892/ol.2018.8767
15. Liu, L., Sun, B., Pedersen, J. N., Aw Yong, K.-M., Getzenberg, R. H., Stone, H. A., & Austin, R. H. (2011). Probing the invasiveness of prostate cancer cells in a 3D microfabricated landscape. *Proceedings of the National Academy of Sciences of the United States of America*, *108*(17), 6853–6856. https://doi.org/10.1073/pnas.1102808108
16. Pienta, K. J., Hammarlund, E. U., Axelrod, R., Amend, S. R., & Brown, J. S. (2020). Convergent Evolution, Evolving Evolvability, and the Origins of Lethal Cancer. *Molecular Cancer Research*, *18*(6), 801–810. https://doi.org/10.1158/1541-7786.MCR-19-1158
17. Pienta, K. J., Hammarlund, E. U., Austin, R. H., Axelrod, R., Brown, J. S., & Amend, S. R. (2020). Cancer cells employ an evolutionarily conserved polyploidization program to resist therapy. *Seminars in Cancer Biology*, S1044579X20302546. https://doi.org/10.1016/j.semcancer.2020.11.016
18. Pienta, K. J., Hammarlund, E. U., Axelrod, R., Brown, J. S., & Amend, S. R. (2020). Poly-aneuploid cancer cells promote evolvability, generating lethal cancer. *Evolutionary Applications*, *13*(7), 1626–1634. https://doi.org/10.1111/eva.12929
19. Pienta, K. J., Hammarlund, E. U., Axelrod, R., Amend, S. R., & Brown, J. S. (2020). Convergent Evolution, Evolving Evolvability, and the Origins of Lethal Cancer. *Molecular Cancer Research*, *18*(6), 801–810. https://doi.org/10.1158/1541-7786.MCR-19-1158
20. Moore, M., Sebastian, J., & Kolios, M. (2019). Determination of cell nucleus-to-cytoplasmic ratio using imaging flow cytometry and a combined ultrasound and photoacoustic technique: A comparison study. *Journal of Biomedical Optics*, *24*, 1. https://doi.org/10.1117/1.JBO.24.10.106502
21. Kostecka, L. G., Pienta, K. J., & Amend, S. R. (2021). Polyaneuploid Cancer Cell Dormancy: Lessons From Evolutionary Phyla. *Frontiers in Ecology and Evolution*, *9*, 660755. https://doi.org/10.3389/fevo.2021.660755
22. Paweletz, N. (2001). Walther Flemming: Pioneer of mitosis research. *Nature Reviews Molecular Cell Biology*, *2*(1), 72–75. https://doi.org/10.1038/35048077
23. Uzbekov, R. & Prigent, C. A Journey through Time on the Discovery of Cell Cycle Regulation. *Cells* **11**, 704 (2022).
24. Collins, K., Jacks, T., & Pavletich, N. P. (n.d.). *The cell cycle and cancer*. 3.
25. Chapter 40 - 43, Editor(s): Thomas D. Pollard, William C. Earnshaw, Jennifer Lippincott-Schwartz, Graham T. Johnson, Cell Biology (Third Edition), Elsevier, 2017, Pages 697 - 754, ISBN 9780323341264
26. Casimiro, M. C., Crosariol, M., Loro, E., Li, Z., & Pestell, R. G. (2012). Cyclins and Cell Cycle Control in Cancer and Disease. *Genes & Cancer*, *3*(11–12), 649–657. https://doi.org/10.1177/1947601913479022
27. Alberts, B., Johnson, A., Lewis, J., Raff, M., Roberts, K., & Walter, P. (2002). Intracellular Control of Cell-Cycle Events. *Molecular Biology of the Cell. 4th Edition*. https://www.ncbi.nlm.nih.gov/books/NBK26856/
28. Barnum, K. J., & O'Connell, M. J. (2014). Cell Cycle Regulation by Checkpoints. *Methods in Molecular Biology (Clifton, N.J.)*, *1170*, 29–40. https://doi.org/10.1007/978-1-4939-0888-2_2

29. Marescal, O., & Cheeseman, I. M. (2020). Cellular Mechanisms and Regulation of Quiescence. *Developmental Cell*, *55*(3), 259–271. https://doi.org/10.1016/j.devcel.2020.09.029
30. Panková, K., Rösel, D., Novotný, M., & Brábek, J. (2010). The molecular mechanisms of transition between mesenchymal and amoeboid invasiveness in tumor cells. *Cellular and Molecular Life Sciences: CMLS*, *67*(1), 63–71. https://doi.org/10.1007/s00018-009-0132-1
31. Paluch, E. K., Aspalter, I. M., & Sixt, M. (2016). Focal Adhesion–Independent Cell Migration. *Annual Review of Cell and Developmental Biology*, *32*(1), 469–490. https://doi.org/10.1146/annurev-cellbio-111315-125341
32. Ananthakrishnan, R., & Ehrlicher, A. (2007). The Forces Behind Cell Movement. *International Journal of Biological Sciences*, 303–317. https://doi.org/10.7150/ijbs.3.303
33. Yamada, K. M., & Sixt, M. (2019). Mechanisms of 3D cell migration. *Nature Reviews Molecular Cell Biology*, *20*(12), 738–752. https://doi.org/10.1038/s41580-019-0172-9
34. O'Neill, P. R., Castillo-Badillo, J. A., Meshik, X., Kalyanaraman, V., Melgarejo, K., & Gautam, N. (2018). Membrane Flow Drives an Adhesion-Independent Amoeboid Cell Migration Mode. *Developmental Cell*, *46*(1), 9-22.e4. https://doi.org/10.1016/j.devcel.2018.05.029
35. Cell Culture Basics Handbook, Gibco™ Education, thermofisher.com/gibcoeducation
36. Audoin, M., & Jauffred, L. (n.d.). *Influence of spheroid on migration of individual glioblastoma cells through extracellular matrix*. 62.
37. Nousi, A. (n.d.). *Optical clearing and invasion/migration study using glioblastoma multiforme spheroids*. 111.
38. Bian, X., Kim, C., & Karniadakis, G. E. (2016). 111 years of Brownian motion. *Soft Matter*, *12*(30), 6331–6346. https://doi.org/10.1039/C6SM01153E
39. Sun, H., Chen, W., Sheng, H., & Chen, Y. (2010). On mean square displacement behaviors of anomalous diffusions with variable and random orders. *Physics Letters A*, *374*(7), 906–910. https://doi.org/10.1016/j.physleta.2009.12.021
40. Nousi, A., Søgaard, M. T., Audoin, M., & Jauffred, L. (2021). Single-cell tracking reveals super-spreading brain cancer cells with high persistence. *Biochemistry and Biophysics Reports*, *28*, 101120. https://doi.org/10.1016/j.bbrep.2021.101120
41. Boal, D. (n.d.). *Mechanics of the Cell: Second edition*. 624.
42. Sommer, C., Straehle, C., Kothe, U., & Hamprecht, F. A. (2011). Ilastik: Interactive learning and segmentation toolkit. *2011 IEEE International Symposium on Biomedical Imaging: From Nano to Macro*, 230–233. https://doi.org/10.1109/ISBI.2011.5872394
43. Schindelin, J., Arganda-Carreras, I., Frise, E., Kaynig, V., Longair, M., Pietzsch, T., Preibisch, S., Rueden, C., Saalfeld, S., Schmid, B., Tinevez, J.-Y., White, D. J., Hartenstein, V., Eliceiri, K., Tomancak, P., & Cardona, A. (2012). Fiji: An open-source platform for biological-image analysis. *Nature Methods*, *9*(7), 676–682. https://doi.org/10.1038/nmeth.2019
44. **Maury**, P., Porcel, E., Mau, A., Lux, F., Tillement, O., Mahou, P., Schanne-Klein, M.-C., & Lacombe, S. (2021). Rapid Evaluation of Novel Therapeutic Strategies

Using a 3D Collagen-Based Tissue-Like Model. *Frontiers in Bioengineering and Biotechnology*, *9*, 574035. https://doi.org/10.3389/fbioe.2021.574035

45. **Muangsanit**, P., Day, A., Dimiou, S., Ataç, A. F., Kayal, C., Park, H., Nazhat, S. N., & Phillips, J. B. (2020). Rapidly formed stable and aligned dense collagen gels seeded with Schwann cells support peripheral nerve regeneration. *Journal of Neural Engineering*, *17*(4), 046036. https://doi.org/10.1088/1741-2552/abaa9c
46. **O'Rourke**, C., Drake, R. A., Cameron, G. W., Jane Loughlin, A., & Phillips, J. B. (2015). Optimising contraction and alignment of cellular collagen hydrogels to achieve reliable and consistent engineered anisotropic tissue. *Journal of Biomaterials Applications*, *30*(5), 599–607. https://doi.org/10.1177/0885328215597818
47. **Sanen**, K., Paesen, R., Luyck, S., Phillips, J., Lambrichts, I., Martens, W., & Ameloot, M. (2016). Label-free mapping of microstructural organisation in self-aligning cellular collagen hydrogels using image correlation spectroscopy. *Acta Biomaterialia*, *30*, 258–264. https://doi.org/10.1016/j.actbio.2015.10.047
48. Wullkopf, L., West, A.-K. V., Leijnse, N., Cox, T. R., Madsen, C. D., Oddershede, L. B., & Erler, J. T. (2018). Cancer cells' ability to mechanically adjust to extracellular matrix stiffness correlates with their invasive potential. *Molecular Biology of the Cell*, *29*(20), 2378–2385. https://doi.org/10.1091/mbc.E18-05-0319
49. Butler, G., Keeton, S. J., Johnson, L. J., & Dash, P. R. (2020). A phenotypic switch in the dispersal strategy of breast cancer cells selected for metastatic colonization. *Proceedings of the Royal Society B: Biological Sciences*, *287*(1940), 20202523. https://doi.org/10.1098/rspb.2020.2523
50. Bouhlel, W., Kui, J., Bibette, J., & Bremond, N. (2022). Encapsulation of Cells in a Collagen Matrix Surrounded by an Alginate Hydrogel Shell for 3D Cell Culture. *ACS Biomaterials Science & Engineering*, *8*(6), 2700–2708. https://doi.org/10.1021/acsbiomaterials.1c01486
51. Lam, D., Enright, H. A., Peters, S. K. G., Moya, M. L., Soscia, D. A., Cadena, J., Alvarado, J. A., Kulp, K. S., Wheeler, E. K., & Fischer, N. O. (2020). Optimizing cell encapsulation condition in ECM-Collagen I hydrogels to support 3D neuronal cultures. *Journal of Neuroscience Methods*, *329*, 108460. https://doi.org/10.1016/j.jneumeth.2019.108460
52. Yeung, P., Cheng, K. H., Yan, C. H., & Chan, B. P. (2019). Collagen microsphere based 3D culture system for human osteoarthritis chondrocytes (hOACs). *Scientific Reports*, *9*(1), 12453. https://doi.org/10.1038/s41598-019-47946-3
53. Sodek, K. L., Brown, T. J., & Ringuette, M. J. (2008). Collagen I but not Matrigel matrices provide an MMP-dependent barrier to ovarian cancer cell penetration. *BMC Cancer*, *8*(1), 223. https://doi.org/10.1186/1471-2407-8-223
54. Cox, T. R., & Erler, J. T. (2011). Remodeling and homeostasis of the extracellular matrix: Implications for fibrotic diseases and cancer. *Disease Models & Mechanisms*, *4*(2), 165–178. https://doi.org/10.1242/dmm.004077
55. Woringer, M., Izeddin, I., Favard, C., & Berry, H. (2020). Anomalous Subdiffusion in Living Cells: Bridging the Gap Between Experiments and Realistic Models Through Collaborative Challenges. *Frontiers in Physics*, *8*. https://www.frontiersin.org/articles/10.3389/fphy.2020.00134

56. **Haw**, R. T. Y., Tong, C. K., Yew, A., Lee, H. C., Phillips, J. B., & Vidyadaran, S. (2014). A three-dimensional collagen construct to model lipopolysaccharide-induced activation of BV2 microglia. *Journal of Neuroinflammation*, *11*, 134. https://doi.org/10.1186/1742-2094-11-134
57. Spichal, M., & Fabre, E. (2017). The Emerging Role of the Cytoskeleton in Chromosome Dynamics. *Frontiers in Genetics*, *8*. https://doi.org/10.3389/fgene.2017.00060
58. Lomakin, A. J., Cattin, C. J., Cuvelier, D., Alraies, Z., Molina, M., Nader, G. P. F., Srivastava, N., Saez, P. J., Garcia-Arcos, J. M., Zhitnyak, I. Y., Bhargava, A., Driscoll, M. K., Welf, E. S., Fiolka, R., Petrie, R. J., De Silva, N. S., González-Granado, J. M., Manel, N., Lennon-Duménil, A. M., … Piel, M. (2020). The nucleus acts as a ruler tailoring cell responses to spatial constraints. *Science (New York, N.Y.)*, *370*(6514), eaba2894. https://doi.org/10.1126/science.aba2894
59. Artym, V. V., & Matsumoto, K. (2010). Imaging Cells in Three-Dimensional Collagen Matrix. *Current Protocols in Cell Biology / Editorial Board, Juan S. Bonifacino ... [et Al.]*, *CHAPTER*, Unit-10.1820. https://doi.org/10.1002/0471143030.cb1018s48
60. Katt, M. E., Placone, A. L., Wong, A. D., Xu, Z. S., & Searson, P. C. (2016). In Vitro Tumor Models: Advantages, Disadvantages, Variables, and Selecting the Right Platform. *Frontiers in Bioengineering and Biotechnology*, *4*, 12. https://doi.org/10.3389/fbioe.2016.00012
61. Karsdal, M. A. (2016). Introduction. In *Biochemistry of Collagens, Laminins and Elastin* (pp. xix–xxxiv). Elsevier. https://doi.org/10.1016/B978-0-12-809847-9.02001-8
62. Slater, K., Partridge, J., Nandivada, H., & Usa, M. (n.d.). *Tuning the Elastic Moduli of Corning® Matrigel® and Collagen I 3D Matrices by Varying the Protein Concentration*. 8.
63. Kloxin, A. M., Kloxin, C. J., Bowman, C. N., & Anseth, K. S. (2010). Mechanical properties of cellularly responsive hydrogels and their experimental determination. *Advanced Materials (Deerfield Beach, Fla.)*, *22*(31), 3484–3494. https://doi.org/10.1002/adma.200904179
64. Metzler, R., Jeon, J.-H., Cherstvy, A. G., & Barkai, E. (2014). Anomalous diffusion models and their properties: Non-stationarity, non-ergodicity, and ageing at the centenary of single particle tracking. *Physical Chemistry Chemical Physics*, *16*(44), 24128–24164. https://doi.org/10.1039/C4CP03465A
65. Kalpić, D., Hlupić, N., & Lovrić, M. (2011). Student's t-Tests. In M. Lovric (Ed.), *International Encyclopedia of Statistical Science* (pp. 1559–1563). Springer. https://doi.org/10.1007/978-3-642-04898-2_641
66. Nachar, N. (2008). The Mann-Whitney U: A Test for Assessing Whether Two Independent Samples Come from the Same Distribution. *Tutorials in Quantitative Methods for Psychology*, *4*(1), 13–20. https://doi.org/10.20982/tqmp.04.1.p013
67. McLeod, S. A. (2019, May 20). *What a p-value tells you about statistical significance*. Simply Psychology. www.simplypsychology.org/p-value.html.